Utah State University
DigitalCommons@USU

All Graduate Plan B and other Reports | Graduate Studies

8-2021

Exploring Questions of Tectonic Geomorphology in the Bear River Range, Utah Using Terrain Analysis and Reconstruction

Edward M. Grasinger
Utah State University

Follow this and additional works at: https://digitalcommons.usu.edu/gradreports

 Part of the Geology Commons, and the Geomorphology Commons

Recommended Citation

Grasinger, Edward M., "Exploring Questions of Tectonic Geomorphology in the Bear River Range, Utah Using Terrain Analysis and Reconstruction" (2021). *All Graduate Plan B and other Reports*. 1572.
https://digitalcommons.usu.edu/gradreports/1572

This Report is brought to you for free and open access by the Graduate Studies at DigitalCommons@USU. It has been accepted for inclusion in All Graduate Plan B and other Reports by an authorized administrator of DigitalCommons@USU. For more information, please contact digitalcommons@usu.edu.

EXPLORING QUESTIONS OF TECTONIC GEOMORPHOLOGY

IN THE BEAR RIVER RANGE, UTAH

USING TERRAIN ANALYSIS AND RECONSTRUCTION

by

Edward Grasinger

A report submitted in partial fulfillment
of the requirements for the degree

Of

MASTER OF SCIENCE

In

Applied Environmental Geoscience

Approved:

06/11/2021

Joel Pederson, Ph.D.
Major Professor

06/12/2021

Tammy Rittenour, Ph.D.
Committee Member

06/13/2021

Shannon Belmont, M.S.
Committee Member

UTAH STATE UNIVERSITY
Logan, Utah
2021

Copyright © Edward Miles Grasinger 2021

All Rights Reserved

CONTENTS

CHAPTER 1

INTRODUCTION

Despite a long tradition of geologic studies in the region surrounding Utah State University, there remain unexplored questions and unutilized approaches for understanding the landscape evolution of the Bear River Range. A large-scale reconstruction of the East Cache fault system can be useful in estimating the total displacement of the fault, its geologic longevity, and total energy involved. Likewise, an analysis of reach-scale features of the Logan River can explore how tectonics and bedrock type affect the patterns and history of the river. Geographic Information Systems (GIS) software is useful in reconstructing, visualizing, and measuring such geomorphological features and changes in landscapes. The products of this study will help visualize and interpret geomorphic patterns of the East Cache fault and the Logan River and provide teaching tools for USU courses and outreach.

This study focuses on the use of GIS for constructing surfaces, measuring, and visualizing features related to geomorphology. Chapter 2 involves reconstructing local paleotopography of the surface preserved at the base of the Eocene Wasatch Formation and total fault slip along the Bear River Range front. One part of the reconstructed paleotopography represents the floor of the Cache Valley basin and the other represents the capping, middle-Cenozoic erosion surface of the Bear River Range. This leads to a third surface -- the fault-plane representing the offset between these two paleotopographic surfaces. These reconstructed surfaces will be used to analyze the

geometry of total slip on the East Cache fault and determine the fault's surface area to estimate earthquake energy expenditure, the fault's geologic longevity, and the slip rate.

Chapter 3 utilizes GIS tools to determine Logan River topographic metrics and to investigate the river's bedrock and tectonic controls. The Logan River is an antecedent river that forms a canyon through the relatively young, tectonically active Bear River Range. The tectonic activity is presumably focused at the East Cache fault (ECF), which the river crosses at the mouth of Logan Canyon. There are also potentially active faults upstream in the Franklin Basin – Temple Peak region, associated with the Klondike and Temple Ridge faults. How might the uplift and subsidence along these faults influence the Logan River's patterns of sinuosity, steepness, and stream power? A testable hypothesis is that the gradient and stream power of the Logan River are highest and the sinuosity is lowest in reaches of greater tectonic uplift, near the mountain front of the Bear River Range.

CHAPTER 2

RECONSTRUCTING TOTAL SLIP OF THE EAST CACHE FAULT

Introduction

Cache Valley is located in a tectonically active part of the Basin and Range, and earthquakes present a major natural hazard to local inhabitants. Previous work documents two major paleoearthquake events in Cache Valley in recent, Holocene geologic history that have been powerful enough to rupture the surface, form fault scarps, and cause powerful shaking (McCalpin and Forman, 1991). Based on geological records like this, geoscientists can look for patterns of ruptures to understand when and where earthquakes occur. Theoretically, some faults may have "characteristic" earthquakes, which display a consistent amount of displacement during periodic, large earthquake events along a given fault or segment of a fault (Schwartz and Coppersmith, 1984).

In this study, I address questions such as, what is the total slip of the East Cache fault (ECF) over the late Cenozoic? What would the seismic moment, moment magnitude, and earthquake expenditure be for this total slip? How long would it take to create the total slip? To address these, I reconstruct paleosurfaces by different means to determine the geometry of total slip on the East Cache fault (ECF) (Fig. 1). This large-scale reconstruction of the East Cache fault system can be useful in exploring fault scale and history. Assuming the ECF slip is dominated by characteristic, large events, I estimate the geologic longevity of the ECF. Prior work by Oaks and Runnells (1992) recognized the Wasatch Formation as a low-relief paleolandscape marker. And Zuchiewicz and Oaks (1993) conduct an early type of terrain analysis and utilize the

Wasatch Formation as a marker to estimate the slip on the ECF. But the GIS-based approach here is much more involved and data-rich, results in a significantly different estimate of slip, and can better address the faulting and landscape evolution of Cache Valley.

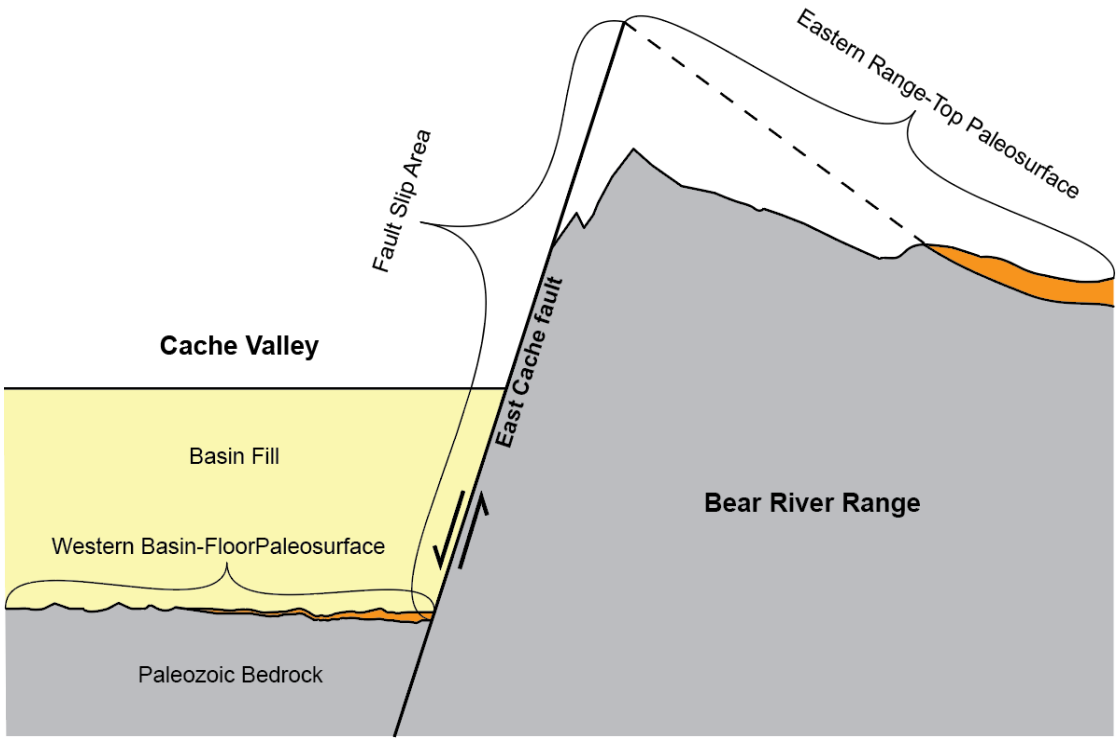

Figure 1. Conceptual cross-section diagram of the total East Cache fault slip and its relation to the reconstructed Wasatch Formation paleosurfaces that it offsets.

Geologic Setting

The Bear River Range and Cache Valley basin are located in northeastern Utah and extend north into southeastern Idaho. The Utah portion of Cache Valley is bounded by the ECF on the east and the West Cache fault to the west. These faults separate the basin from the Bear River Range and Wellsville mountains, respectively. The Cache

Valley basin is capped by Lake Bonneville and younger alluvial deposits, but the deeper basin holds up to ~3655 m of Neogene deposits in the central section of the basin. (Evans and Oaks, 1996). In contrast, Proterozoic and Paleozoic rocks are uplifted in the footwall of the ECF.

The Wasatch Formation is a 110 – 245-meter-thick Paleogene rock unit that is approximately 55 million years old (DeCelles, 1994). The Wasatch was deposited across an erosional surface in Northern Utah and is preserved on the east side of the Bear River Range. The Wasatch consists of poorly-sorted conglomerate, mudstone, siltstone, and minor lacustrine limestone and marl (Oaks and Evans, 1996). The conglomerate interbeds are composed of well-rounded Paleozoic carbonate cobbles and pebbles. The Wasatch is also characterized by abrupt changes in facies and lithologic interfingering. The facies assemblage indicates the Wasatch Formation was formed in an alluvial depositional environment in the past (DeCelles, 1994).

The East Cache fault zone (ECFZ) is approximately 77 kilometers long. It is responsible for the uplift of rock formations including the Wasatch Formation in the footwall. The fault dips 65° to 75°W near the floor of a fault trench excavated in a study along the central segment by McCalpin and Forman (1994), but the dip of the fault near the surface is as little as 45° to 50°W degrees in other segments (Evans and Oaks, 1996). The fault began during the Neogene and has a slipping rate from 0.2 to 1 mm/yr for the Holocene (McCalpin and Forman, 1994). The central segment is the most tectonically active part of the ECF with studied evidence of Holocene earthquake activity. The north and south segments are the least active and only contain known evidence for earthquake activity that dates back to the mid to late Pleistocene (McCalpin and Forman, 1991).

According to McCalpin and Forman (1991), the ECF had two Holocene earthquake events with Richter magnitudes that ranged from 6.6 to 7.1, vertical offsets of 0.8 to 1.9 m, and a recurrence interval of 5.8 ka (minimum) to 11.5 ka (maximum).

Methods

To construct the three-dimensional paleosurface, point elevations from the top of Paleozoic bedrock below the Cache Valley basin and Wasatch Formation outcrops along the backside of the Bear River Range can be used along with interpolation methods. For elevation data, a 10-meter resolution digital elevation model (DEM) from the United States Geological Survey is used, and geological shapefiles of the geologic units and geologic lines in the Bear River Range from the Utah Geological Survey are also used. Another important dataset used is a map that displays elevation contours of the top Paleozoic bedrock under the surface of the Cache Valley basin provided by Robert Oaks, emeritus professor at Utah State University (Fig. 2). The elevation contours in this map are based on isostatic residual gravity data, oil well data, and five seismic-reflection profiles.

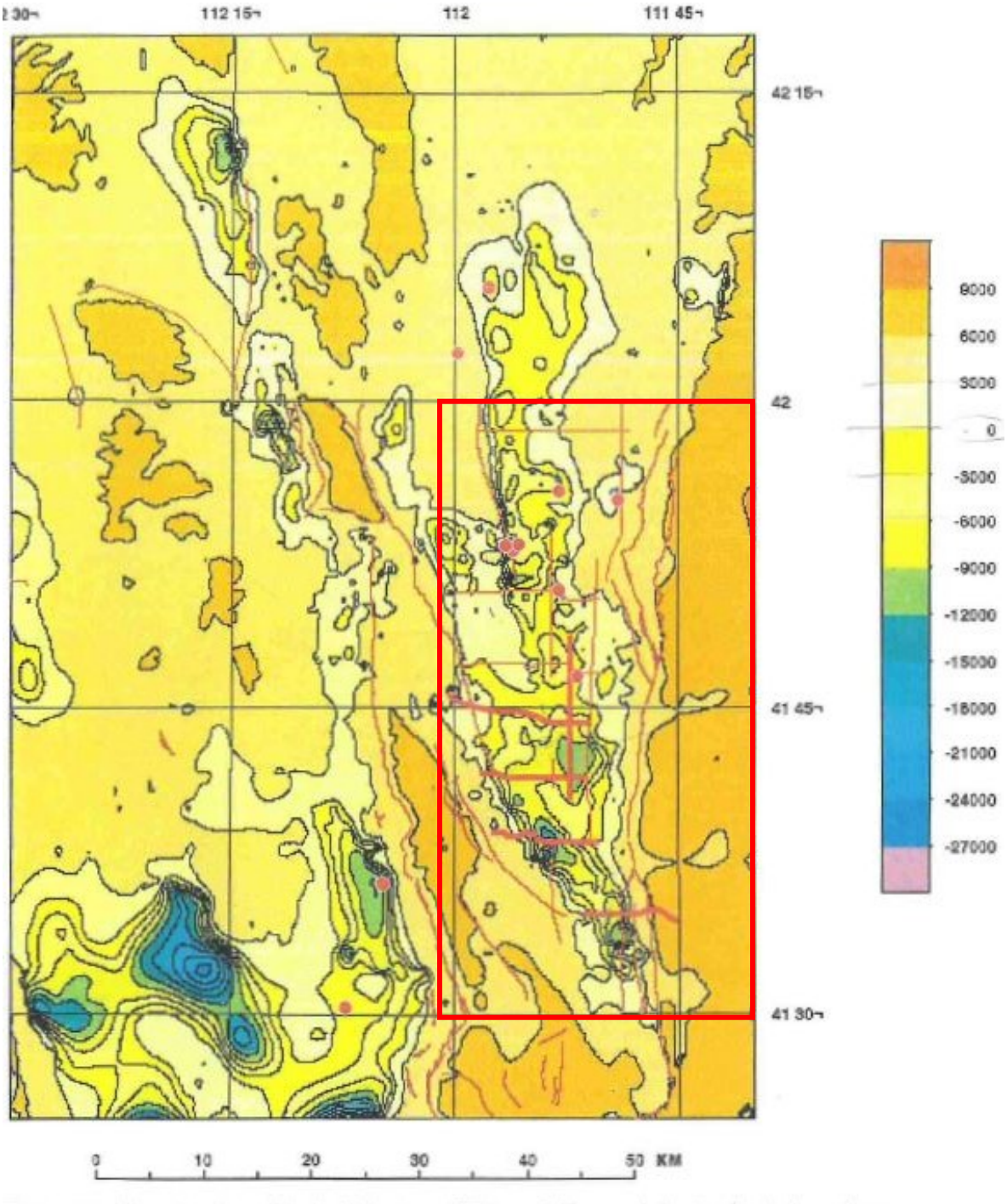

Figure 2. Map that displays the elevation of the top of Paleozoic bedrock determined using residual gravity data with an assumed density contrast of 0.46 g/cm^3, estimated depths from 11 oil wells (red points), and 5 seismic profiles (red lines). The red box represents the Cache Valley Basin region of interest, also shown in Fig. 3. The contour interval is 3000 feet. Data was compiled by Vicki Langenheim and provided by Dr. Robert Oaks.

Paleosurface Elevation Points for Eastern Range-Top

The first step in the analysis was to create elevation points of the basal contact of the Wasatch Formation in the eastern range-top. To do this, the geologic units and geologic contact lines of the Wasatch Formation were extracted from the UGS shapefiles. The *select by attribute* and *select by location* tools were used to export the Wasatch Formation attributes to their own polygon layer and extract the contacts as line shapefiles using the *Polygon to Line* geoprocessing tool. The *Create Point Features Along a Line* tool was used to create points (colored red in Fig. 3) at 1000 m intervals along the contact lines. After the points were created, the *Extract Values to Points* tool was used to add the elevation raster values from the 10-meter DEM.

To extend the eastern range-top paleosurface and project it westward to the ECF, arbitrary points (colored orange in Fig 3.) were created on the eastern range-top based on projected slope estimates of where the Wasatch Formation would be outside of the known Wasatch Formation geologic units. A handful of points were plotted along the eastern end of the ECF. Additional arbitrary points were plotted at the top of modern peaks based on estimates of how high the Wasatch Formation would be if it had not been eroded away from weathering. At the peaks, the height of Wasatch Formation basal contact is presumed to be 50 m higher than the modern elevation of the peaks. The arbitrary points are shown in orange on the map in Fig. 3 with the known eastern range-top points shown in red.

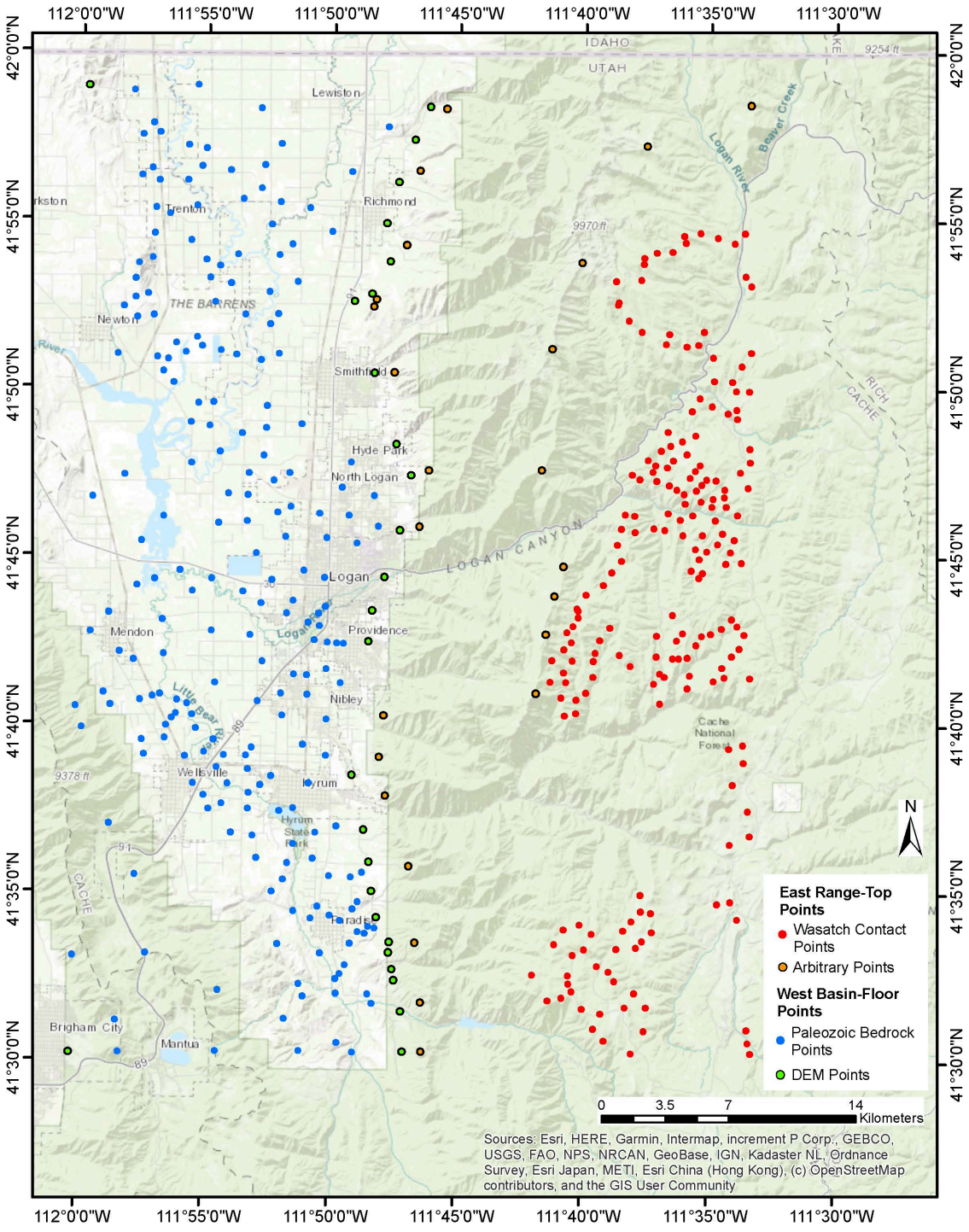

Figure 3. Map displaying the elevation points for the western basin-floor and eastern range-top paleosurfaces.

Paleosurface Z-Values for Western Basin-Floor

To create the western basin-floor paleosurface, the first step was to georeference the Paleozoic bedrock map shown in Figure 1. in *ArcMap*. The map was converted from a PDF to a Tagged Image File Format (TIFF) image, and then the *define projection* tool was used to assign the TIFF the UTM Zone 12N projected coordinate system. The map was then georeferenced by inputting the Universal Transverse Mercator (UTM) coordinates as control points. Points (colored blue in Fig 3.) then were plotted on the contour lines manually and the elevation values of the contours were assigned to those points in the attribute table manually. Using the *Field Calculator*, the elevation values were converted from feet to meters. To have the eastern edge of the paleosurface blend in with the ECFZ and extend the paleosurface at the proper boundaries of the study area, points (colored green in Fig 3.) were plotted manually along a ECF line shapefile and two additional points were plotted in corners at the west edge of the basin-floor. Elevation values from the 10-meter DEM were then added manually to these points.

Interpolating Surfaces

Interpolation methods were explored for creating two surfaces based upon the two sets of elevation points. Four interpolation geoprocessing tools in the spatial analyst were explored: *Inverse Distance Weighting (IDW)*, *Spline*, *Kriging*, and *Natural Neighbor*.

IDW interpolation uses a linearly weighted combination of a collection of sample points in determining cell values. It assumes that the influence of the mapped variable decreases in distance from its point location. The IDW method is suitable when the

number of points is dense enough to interpret the variation in local surface that is essential for the interpolation. The spline method uses an algorithm that keeps surface curvature minimal to determine cell values. The output surface passes through all sample points and approximates valleys and ridges in the sample data. The tension spline option was used, which works with the slope and the slope's rate of change derivatives of the dataset.

The kriging method is distinct, as it performs an interactive investigation of z-value points based on autocorrelation. The distance and direction between points reflects the target spatial correlation used to characterize variation in the surface, and a weighted average method is used to predict cell values based on this. Because this method is designed for when there are directional or spatially correlated trends in data, kriging is commonly used for geologic and soil science applications.

Natural neighbor interpolation applies an algorithm that finds the nearest group of input points to a query point and weighs them based on the balanced areas of Thiessen polygons created around the nearby points to interpolate a value (Fig. 4). It uses the Delauney triangulation when selecting the nearest points for the interpolation. This interpolation works best in cases where z-value points are scattered and unevenly distributed. This method works similarly to the IDW and kriging interpolation because it applies a weighted-average method, but the natural neighbor interpolation differs in that it assigns weight based on the percentage of overlap of Thiessen polygons rather than the distance from the interpolated point. This interpolation method does not take trends into

account and will not extrapolate peaks, valleys, or ridges. Instead, the values of the output raster remain within the value range of the input points (Childs, 2004).

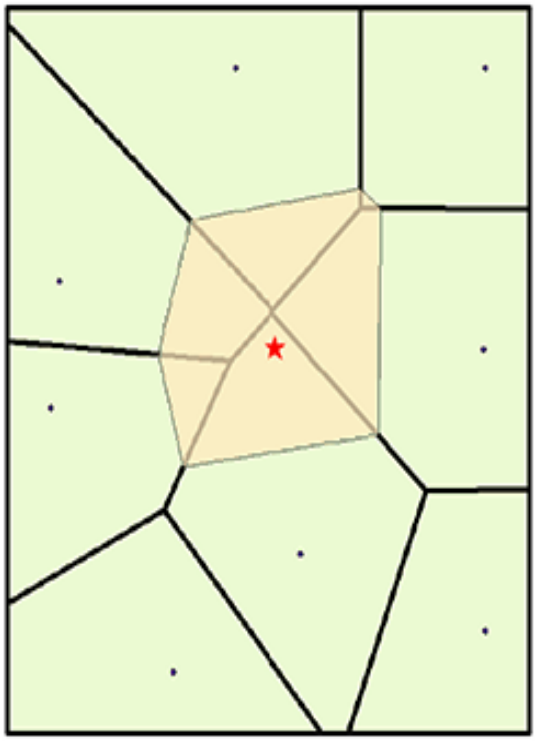

Figure 4. Thiessen polygons (green polygons) are created around neighboring points (black points) of the interpolated point (red star) and a new Thiessen polygon (beige polygon) is created around the sample point. The interpolation is determined based on the weight/percentage of overlap between the newly created Thiessen polygon and initial Thiessen polygons. (Image courtesy of ESRI).

East Cache Fault Projection

A Triangular Irregular Network (TIN) was used to project the ECF as a planar surface. Although normal faults are generally listric, the ECF is being represented as a planar surface due to the limited availability of data and information below the subsurface. TIN surfaces are created by connecting nodes with a set of edges that form a system of triangles. The TIN was chosen to represent the ECF over the interpolation

methods because they keep strictly to the input data and do not interpolate features. Additionally, the TIN surface can be manually edited to have the extension of the ECF projection fit the two paleosurfaces.

To create the TIN surface, line shapefiles of the mapped trace of the ECF were obtained from Utah Automated Geographic Reference Center. The *Select by Attribute* and *Export Data* tools were used to extract the fault lines. Then, the *Create Points Along Lines* tool was used to create points every 250 meters along the line. Next, the *Add XY Coordinates* tool was used to assign X and Y UTM Coordinates to each point. To project the fault line into a planar surface, synthetic points were established 1 km to the east and to the west of the mapped fault trace (Fig. 5). For the points to the east and west, 1000 m was added and subtracted from the original X-coordinates, respectively. The 10-m DEM and the *Extract Values to Points* tool were used to assign elevation values to the associated points along the fault lines. For the east and west sets of points, the *Make XY Event Layer* tool was used to create separate layers which then were made into separate shapefiles by using the *Copy Features* tool. To assign elevations to the synthetic east and west points for the fault surface, the following equation was used to calculate height (h) relative to the true fault trace:

$$h = \tan\theta * 1000 \qquad (1)$$

Based on the previous study of McCalpin and Forman (1991), the angle of the fault plane (θ) was taken to be 65°. Using the *field calculator*, the relative height values to the east and west were an added or subtracted 2144.5 m, respectively.

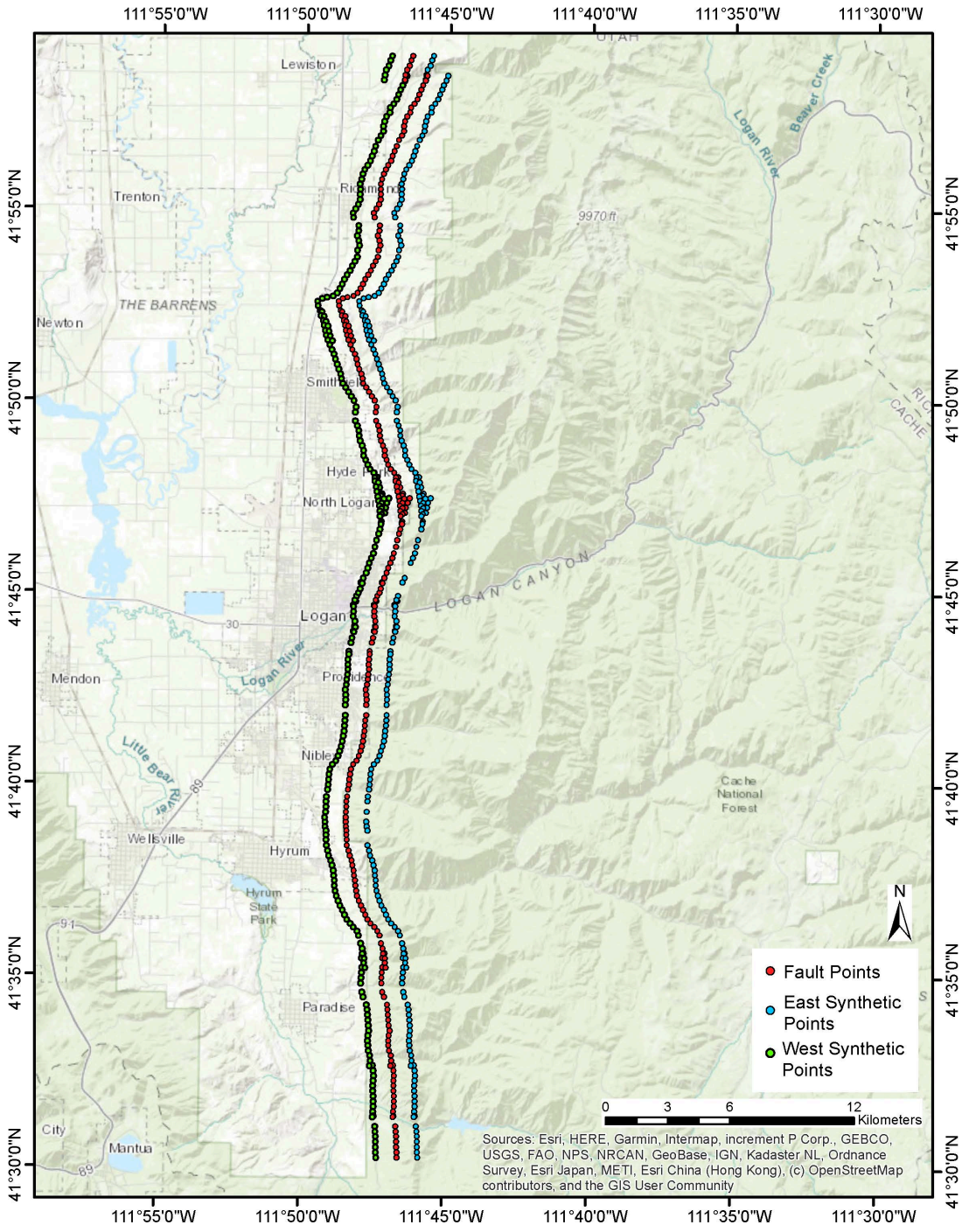

Figure 5. Map that displays the 250-m spaced fault points used to create the TIN fault surface. The east and west synthetic points are 1 km from the fault-trace points.

The *Create TIN* tool was used to construct the fault plane model through the three sets of elevation points. When the TIN was first produced, the surface edges extended far beyond both the elevations of eastern range-top and western basin-floor paleosurfaces. To obtain a more accurate estimate of the total fault slip, the height of the TIN edges were adjusted to approximately match the elevations of both the east and west paleosurface edges oriented towards the TIN. This was done using the interactive *TIN Editing* toolbar to set z-values for the nodes at the east and west edges, which are then used in clipping the TIN surface. Once clipped, the *Add Surface Information* tool was used to calculate the TIN's surface area. The average total slip represented by the TIN was calculated by dividing the TIN surface area by the TIN surface's width.

Earthquake Energy

To explore the implications of the ECF projection, the entire surface of Neogene slip (the clipped TIN) was treated as if it was generated in a single-event earthquake. This is more of a "what-if" analysis to demonstrate how 3D analysis from GIS can be used to estimate seismic moment, moment magnitude, and earthquake energy release of fault zone. Seismic moment (M_o) is a measure of the size of an earthquake based on the area of the fault rupture, the displacement of the fault slip, and the rigidity of the rock along the fault plane.

$$M_o = Area * Slip * Rigidity \quad (2)$$

M_o is not a measure of energy, but it is rather a measure of stress released during an earthquake. Because most of the rocks along the fault plane consist of limestones and

some crystalline rocks, the rigidity was assumed to be in the range of 2×10^{10} to 5×10^{10} Pa (Turcotte and Schubert, 2002).

After determining the seismic moment, the moment magnitude ($M_{w)}$ can be estimated (Hanks and Kanamori, 1979). Similar to Richter's local magnitude scale, the moment magnitude ranges from 1 to 10 on a logarithmic scale. When using dyne-centimeters, the equation for determining moment magnitude is:

$$M_w = 2/3 \log_{10}(M_o) - 6.05 \quad (3)$$

From knowing the moment magnitude of an earthquake, the energy expenditure (in joules) from an earthquake event can be estimated by:

$$Log\ E = 5.24 + 1.44M_w \quad (4)$$

Results and Discussion

Interpolated Paleosurfaces

From the four interpolation methods explored for non-planar paleosurfaces, the natural neighbor approach appears to have the best output for both surfaces based on the elevation point distribution and the fact that this interpolation method stays true to the input data (Table 1). The natural neighbor interpolation's values did not exceed the maximum and minimum elevation values in the point data.

TABLE 1. INTERPOLATION STATISTICS FOR THE EASTERN RANGE-TOP AND WESTERN BASIN-FLOOR PALEOSURFACES

Raster	Mean Elevation (m)	Maximum Elevation (m)	Minimum Elevation (m)	Standard Deviation
Western Basin-Floor				
10-meter DEM	1,484	2,658	1,330	182
IDW	75	1,829	-3,653	1080
Spline	699	14,280	-4,347	2,002
Kriging	-154	1,580	-2,985	919
Natural Neighbor	285	1,829	-3,655	1,219
Eastern Range-Top				
10-meter DEM	2,134	3,041	1,425	287
IDW	2,540	3,950	1,730	555
Spline	2,705	4,086	1,693	652
Kriging	2,658	3,948	1,734	618
Natural Neighbor	2,670	3,950	1,730	606

The IDW interpolation yielded similar statistics to the natural neighbor interpolation. However, the unequal distribution of elevation points on both paleosurfaces caused the IDW interpolation to create unexpected peaks and pits around some points. The IDW method works best when the elevation points are evenly distributed. The spline

approach yielded maximum and minimum values that are beyond the range of the actual elevation values (Table 1). The spline method minimizes surface curvature that creates a smoothing effect that causes interpolation values to be a lot higher or lower than the true values of the sample points. Spline is not the appropriate interpolation in this case because the values of elevation points differ drastically in some regions and are too close together. Like the spline, the kriging interpolation gave interpolation values that are higher and lower than the actual elevation values. Kriging can be a good choice for making predictions when creating a surface, but the interpolation does not pass through the sampling points and the interpolated values do not stay true to the range of the actual elevation values.

In the western basin-floor paleosurface, to the left in Figure 6, the maximum and mean elevation of the basin-floor is -3,655 m and 285 m, respectively. The basin-floor paleosurface created from the natural neighbor interpolation appears to follow the pattern of contours in Figure 1. In both maps, they have the same four distinct regions where the basin is very deep (< -2,700 m) located in the central area of the basin-floor. The eastern edge at the ECF and the southwestern area at the Wellsville range of the basin-floor paleosurface represent modern elevations.

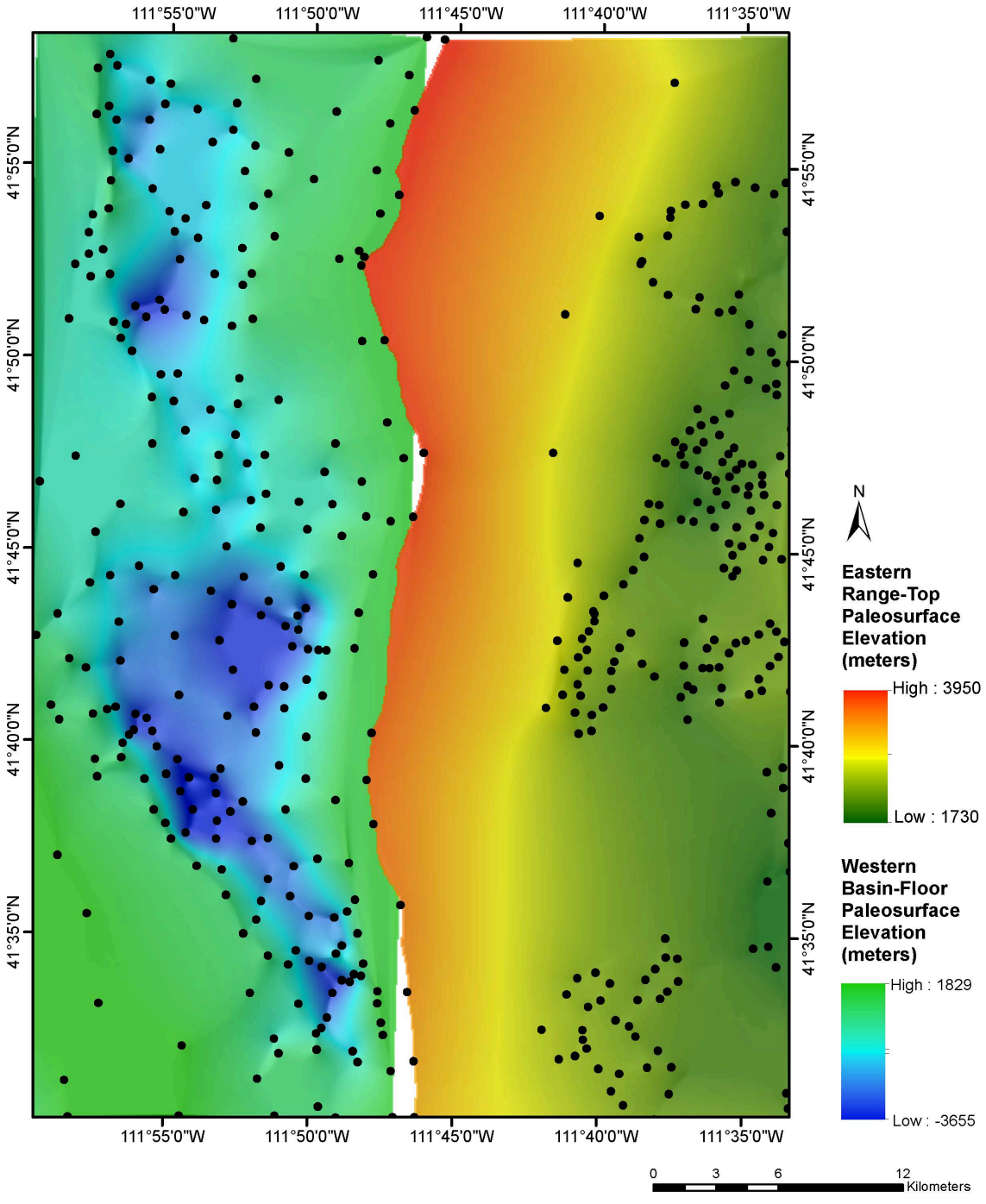

Figure 6. A map view of the two paleosurfaces created with hillshade by an interpolation of points using the natural neighbor method. The area on the left displays the paleosurface of the western basin-floor and the area on the right displays the paleosurface of the eastern range-top. The black dots represent the interpolation points used to create the paleosurfaces.

The interpolated eastern range-top paleosurface, to the right in Figure 6, is primarily planar in shape. The range-top paleosurface has a maximum elevation of 3,950 m at the northwestern edge of the mountain front, a minimum elevation of 1,730 m at the mountain side, and a mean elevation of 2,670 m. The western region of the paleosurface is drastically higher than the modern topography of the Bear River Range mountain front (Fig. 7). The Wasatch Formation basal contact is mostly preserved in the mountain side of the Bear River Range, but the contact has been eroded away by weathering in the mountain front area (Fig. 6A). The arbitrary points that were created to extend the interpolated surface westward are a major source of uncertainty. The points were estimated based on slope values from the preserved basal Wasatch Fm. contact, and the exact elevation of this basal contact in the eastern and northern portions of the eastern range-top paleosurface is unknown.

A

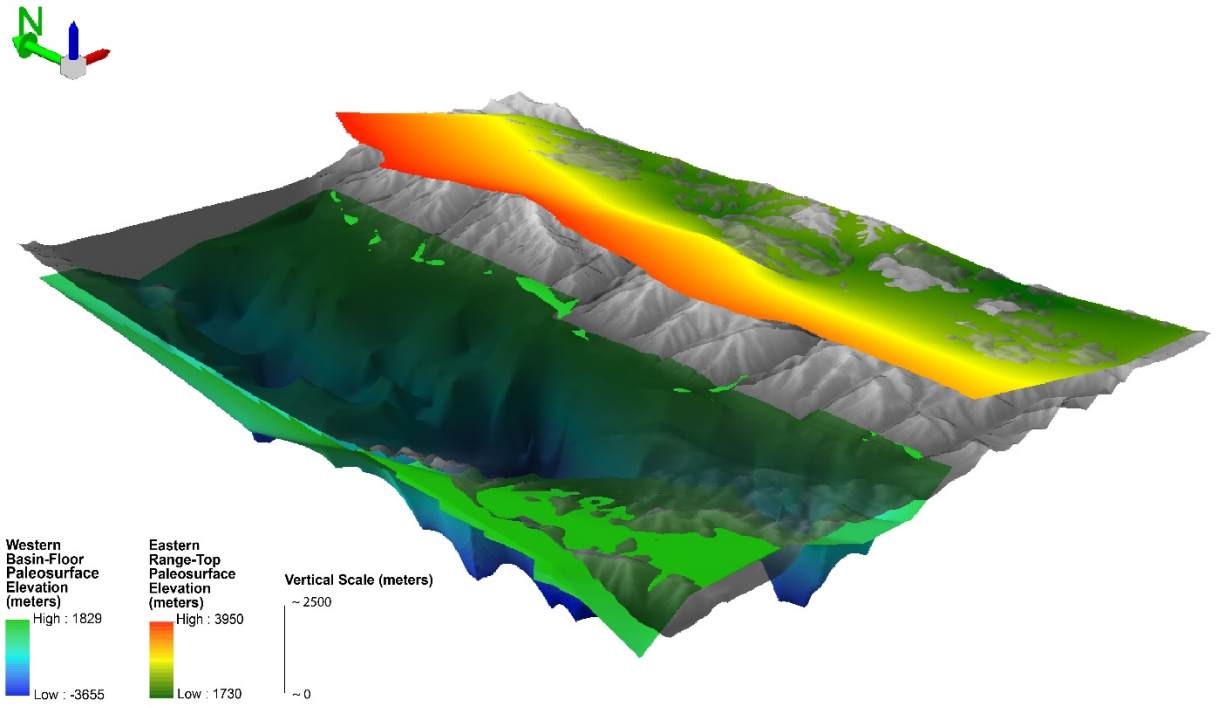
N
Western Basin-Floor Paleosurface Elevation (meters)
High : 1829
Low : -3655
Eastern Range-Top Paleosurface Elevation (meters)
High : 3950
Low : 1730
Vertical Scale (meters)
~ 2500
~ 0

B

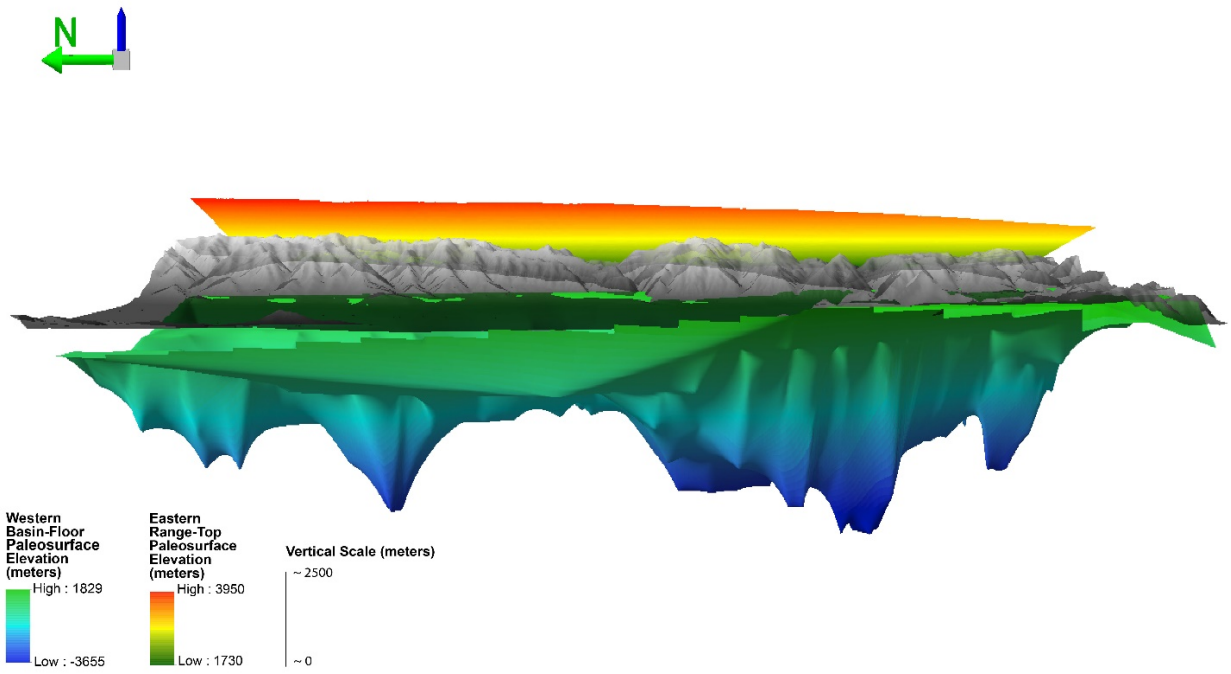

Figure 7. A) 3D display of the two paleosurface models created in ArcScene relative to the modern topography of Cache Valley and the Bear River Range. The model to the left represents the top of the paleozoic bedrock on the western basin-floor and the model to the right represents the Wasatch Fm. paleosurface of the Bear River Range to the east. B) Horizontal view of the paleosurfaces with respect to the modern topography looking straight east.

East Cache Fault Projection

As displayed by Figure 8, the ECF TIN has an almost vertical orientation and undulates from north to south. It also has a ribbed and striated texture. The upper edge of the TIN is smooth because it was clipped to match the relatively smooth east range-top paleosurface. The bottom of the TIN is more irregular due to the high contrast in depth along the length of the basin-floor paleosurface. The TIN appears to align and blend in perfectly with the two paleosurfaces, as seen from a bird's eye view (Fig. 9A). Looking at the ECF TIN with the paleosurfaces from an east-west cross-sectional vantage in Figure

9B, the ECF TIN's dip appears to be 65°. Realistically, the ECF is listric in shape and it even has 50° dips at the land surface at the south end of the fault (Evans and Oaks, 1996). Therefore, the constant-dip assumption is too steep to match the true pattern in the subsurface and explains why the ECF TIN does not contact the east edge of the basin-floor.

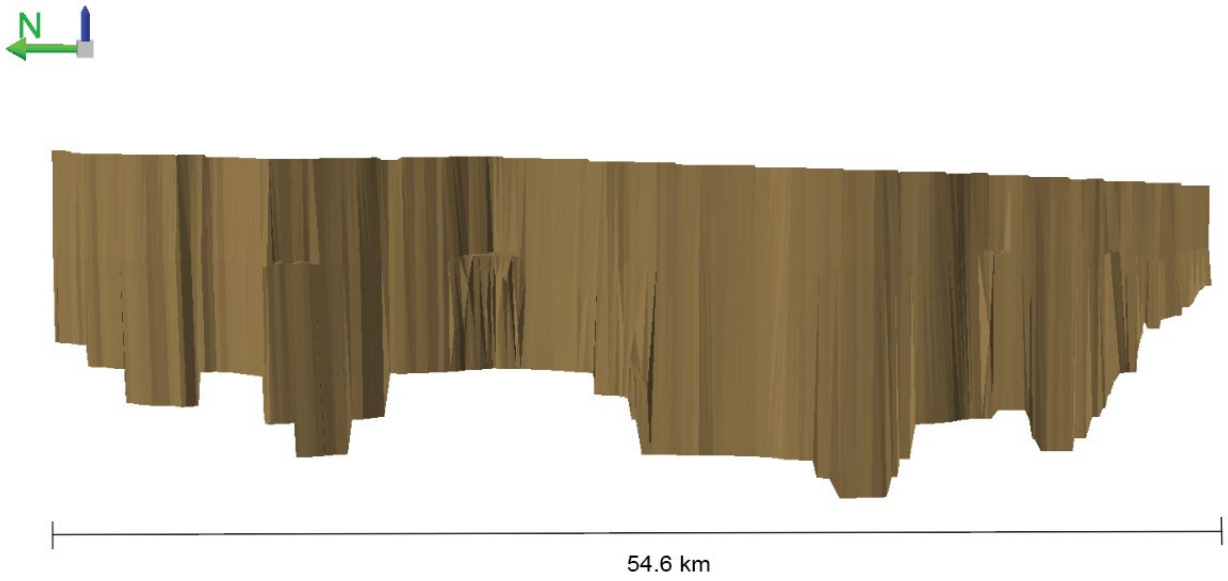

Figure 8. 3D view of the East Cache fault TIN, looking straight east.

A

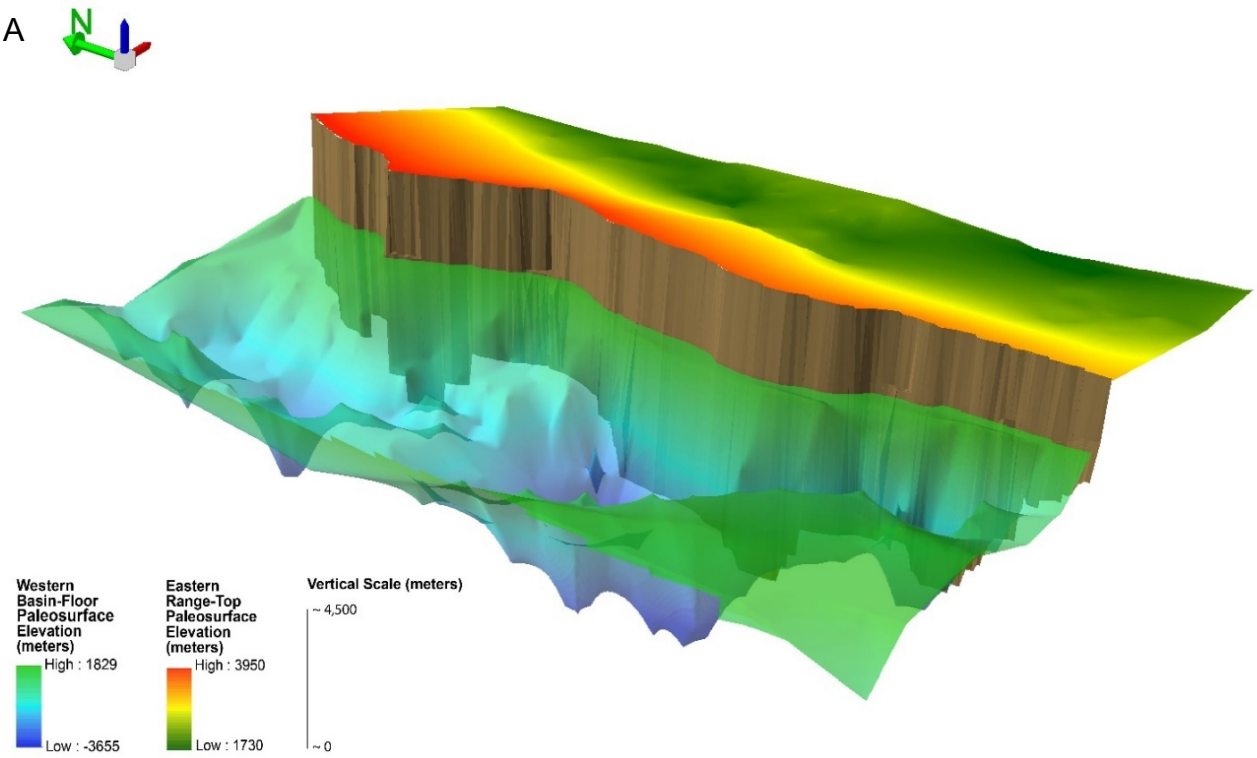
N
Western Basin-Floor Paleosurface Elevation (meters)
High : 1829
Low : -3655
Eastern Range-Top Paleosurface Elevation (meters)
High : 3950
Low : 1730
Vertical Scale (meters)
~ 4,500
~ 0

B

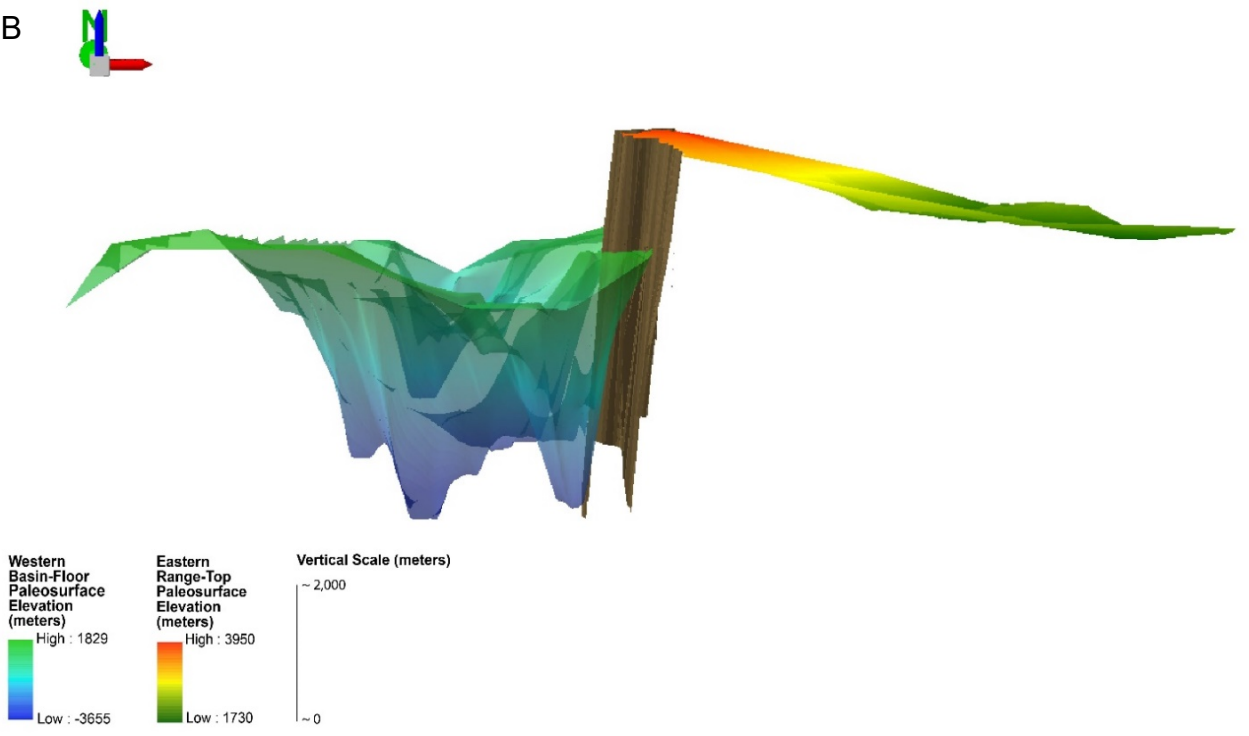
N
Western Basin-Floor Paleosurface Elevation (meters)
High : 1829
Low : -3655
Eastern Range-Top Paleosurface Elevation (meters)
High : 3950
Low : 1730
Vertical Scale (meters)
~ 2,000
~ 0

Figure 9 (previous page). A) 3D representation of the ECF TIN and the interpolated paleosurfaces from birds-eye view looking northeast. B) Cross-sectional view of the same reconstructed surfaces looking directly north.

The surface area of the ECF TIN is 316,346,167 m^2, and the maximum and minimum elevation of the ECF TIN is 4,000 m and -3,655 m, respectively. From the *Calculate Geometry* tool, the length measured from north to south along the undulating trace of the ECF TIN surface is 54,645 m, and thus the calculation of the fault's average slip or displacement is 5,790 m. In their 1993 study, Zuchiewicz and Oaks make an analogous, but more simple, linear estimate of the total "uplift" of the Bear River Range using the Wasatch Fm. Their estimate was 3744 m at the mountain front, more than 2000 meters less than the result here. This is mostly because their estimate of the Cache Valley basin depth is significantly less than used in this analysis.

Based on the surface area of the ECF TIN, ~2/5 of the ECF TIN surface area is created from uplift of the foot wall and ~3/5 of the surface area below the surface is created from subsidence. From measuring average elevations of the ECF TIN above and below the modern surface, ~1/3 of the fault slip is expressed as uplift of the footwall while ~2/3 is expressed as subsidence. These results are consistent with observations that the majority of the absolute elevation changes normal-fault earthquakes occurs as coseismic subsidence, while less is uplift of the footwall (Stein and Barrientos, 1985).

From McCalpin and Forman (1991), the displacement caused by a single characteristic earthquake of the ECF ranges from 0.8 to 1.9 meters, and the recurrence interval between earthquake events ranges from 5.8 to 11.5 ky. Given these values, Table 2 reports how many earthquake events and how much time it would take to create the

reconstructed full ECF offset. The number of earthquake events needed to create the total displacement ranges from 3,047 to 7,238 events, and the time to create that amount of total displacement ranges from 17.7 to 83.2 million years. These estimates are greater than expected. Instead, the sequence of geologic relations in our region indicates the ECF should be ~5 million years old (Susanne Janekce and Bob Oaks, pers. comm., October 2020). Therefore, even the minimum-age is apparently about 3.5 times too long.

TABLE 2. NUMBER OF EARTHQUAKES AND TIME NEEDED TO CREATE TOTAL ECF DISPLACEMENT

	Minimum	Maximum
Total Slip/Displacement	5,790 m	
Recurrence Interval	5,800 years	11,500 years
Displacement per Event	1.9 m	0.8 m
Number of Earthquakes	3,047	7,238
Years to create displacement	17,672,600	83,237,000

What might explain this large discrepancy in expected results? A critical assumption made in using earthquake-event values from the McCalpin and Forman (1991) study is that the total geologic slip over time was created only from large, ~6 to 7 magnitude, characteristic earthquakes that happen several thousand years apart and

rupture the ground surface. Not all earthquakes and fault slip occur in the very largest earthquakes. In fact, this analysis ignores most of the earthquakes and the creep that happens more frequently and contribute to the fault's total slip over time. The Gutenberg-Richter law in seismology shows a negative power-law relation between the magnitude and number of earthquake events (Gutenberg and Richter, 1944). This indicates that the vast majority of earthquake events on a fault are relatively small in magnitude, while large magnitude earthquakes occur rarely. If we assume the ECF is ~5 million years of age and the recurrence interval is the shorter estimate from McCalpin and Forman (1991) of 5,800 years and recognize that the ECF TIN surface area is 3.5 times greater than it should be, we can presume that 30% (or 1/3.5) of the total slip is from the large, rare characteristic earthquakes, while 70% of the total slip is from the much more numerous, smaller earthquake events and creep over those 5 million years.

Earthquake Energy

To gain an appreciation for how much energy has been expended in mountain building in our region, one can pretend that the entire slip of the ECF over time occurred in one huge event and compare that to other events. Table 3 displays the estimates for the seismic moment, moment magnitude, and energy expenditure based on the TIN's surface area, total displacement, and shear modulus. The maximum rigidity value of 4×10^{10} Pa is our preferred option because the ECF mostly penetrates below the basin and consists mostly of crustal rocks along the fault's path. Therefore, the magnitude of the TIN's single earthquake event is 9.2 and the energy release is 3.1×10^{18} J.

TABLE 3. EARTHQUAKE ENERGY METRICS

	Limestone (Minimum)	Basement (Maximum)
ECF TIN Surface Area	316,346,167 m^2	
Rigidity	2 x 10^{10} Pa	4 x 10^{10} Pa
Seismic Moment (M_o)	3.66 x 10^{22} Nm	7.33 x 10^{22} Nm
Moment Magnitude (M_w)	9.0	9.2
Energy Expenditure	1.58 x 10^{18} Joules	3.08 x 10^{18} Joules

To get a sense for how much energy the total ECF slip represents, compared to historic earthquakes, a 9.2 magnitude is very extreme and occurs seldomly. A couple examples of historical magnitude 9 earthquakes include the 2011 Tōhoku earthquake and the 2004 Sumatra earthquake. However, rather than a normal fault, both earthquakes occurred on subduction-zone thrust faults and were powerful enough to trigger huge tsunamis that devastated coastal regions and led to several thousands of casualties. In another example, the energy release of 3.1 x 10^{18}J for the total ECF slip is approximately 200,000 times the amount of energy released by the Hiroshima atomic bomb.

In the introduction, research questions were posed about the total slip of the ECF as well as the seismic moment, moment magnitude, energy expenditure, and geologic longevity of the ECF slip. After the analysis, these questions are answered as if they occurred in one single earthquake event. Although this exercise is treating the creation of

the ECF as a single earthquake event, its formation took several earthquake events. A 9.0 magnitude earthquake is not realistic for a normal fault like the ECF and occurs on larger-scale megathrust fault systems. This exercise is a "what-if" analysis to estimate fault displacement and earthquake metrics using GIS. The largest uncertainty and source of error for this exercise is not knowing the exact elevation of the Wasatch Formation basal contact before it eroded away. It is possible that the east range-top paleosurface was estimated too high and therefore the estimates of total displacement, surface area, seismic moment, moment magnitude, and earthquake energy expenditure of the ECF TIN are too high. In future studies, this exercise can be improved by performing this analysis based on multiple events, multiple segments, and taking into account the different dip angles associated with each segment. Additionally, more information and data of the ECF subsurface may be useful in obtaining more accurate results.

CHAPTER 3

LOGAN RIVER PATTERNS

Introduction

This project observes and measures features of the longitudinal profile of the Logan River, including the river's unit stream power, which is a particularly useful metric for examining landscape evolution and river incision. Mackin (1948) stated that a "graded" or equilibrium stream has its gradient adjusted everywhere along its length to combine with discharge and provide the necessary energy to transport bedload downstream. The energy required to transport bedload, or erode bedrock, can be measured as stream power. Considering this idea of an equilibrium stream, what would be the corresponding equilibrium form of the profile of the Logan River? For most rivers, including the Logan River, discharge increases downstream. And bed grainsize decreases downstream in well-adjusted streams. Both of those trends dictate that gradient should decrease smoothly downstream, forming an equilibrium profile. Considering that stream power is the product of discharge and slope, stream power should remain relatively constant, or only change smoothly, because as the gradient decreases downstream, the discharge increases. Likewise, as bed grainsize decreases downstream, gradient will decrease to just what is needed to transport increasingly fine sediments (Mackin, 1948).

These are the theoretical reasons why an ideal river profile should be smooth and decrease in gradient as it flows downstream. But in the case of the Logan River, the profile is not this simple. Stream power and the longitudinal profile are conceptually important for documenting where and investigating why variations or anomalies exist.

An analysis of reach-scale features of the Logan River can explore how tectonics and bedrock type may affect the patterns and history of the river. In a USU Master's Thesis, DeGraff (1976) plotted the long-profiles of several drainages in the Bear River Range, including the Logan River. The analysis here with GIS tools is distinct because it is focused on the Logan River and on calculating several metrics along its length. By determining the unit stream power, we can determine the river's potential for bedload transport or erosion and deposition per unit area of its bed along the stream. Research questions for this exercise include: 1) Where is sinuosity highest and what might it tell us about the history and evolution of the Logan River? 2) Where are gradient and stream power highest and what are the causes? 3) Is there a correspondence with bedrock type and sinuosity, canyon-bottom width, gradient, or stream power? To answer these questions, I will be using GIS to measure and compare these metrics and patterns along the Logan River. In this study, it is predicted that unit stream power will be highest in the reaches affected by tectonic uplift and hard bedrock and lowest in broader valley reaches and weaker bedrock.

Geologic Setting

The upper Logan River study watershed is 556 km^2 in area and 55 km long down to first dam at the mouth of Logan Canyon (Fig. 1). The river begins in alpine catchments and springs feeding Franklin Basin, which straddles at the Idaho-Utah border. As the river flows downstream through Franklin Basin, it follows the Klondike fault until river-km 14, and the surrounding bedrock starts off in Ordovician St. Charles, Swan Peak Quartzitie, and Garden City Formations (Fig. 2). These units are primarily limestone and dolostone with some having interbeds of conglomerate, breccia, and sandstone. The river encounters Quaternary moraine and till units at river-km 8 and again at river-km 12. At river-km 11 to 12 (Fig. 2), the river gets to Cambrian bedrock, which consist of interbedded limestone and dolostone with shale and siltstone from the Bloomington Formation and Blacksmith Dolomite. At river-km 16, the bedrock type transitions to Tertiary Wasatch Formation, which is composed of poorly sorted conglomerate, siltstone, and interbeds of limestone and marl. Here, the Logan River conflues with Beaver Creek. From river-km 18 to 23, the river flows through a broad valley of Wasatch sitting on Cambrian bedrock and Tony Grove Creek joins the Logan River around river-km 20 (Fig. 2).

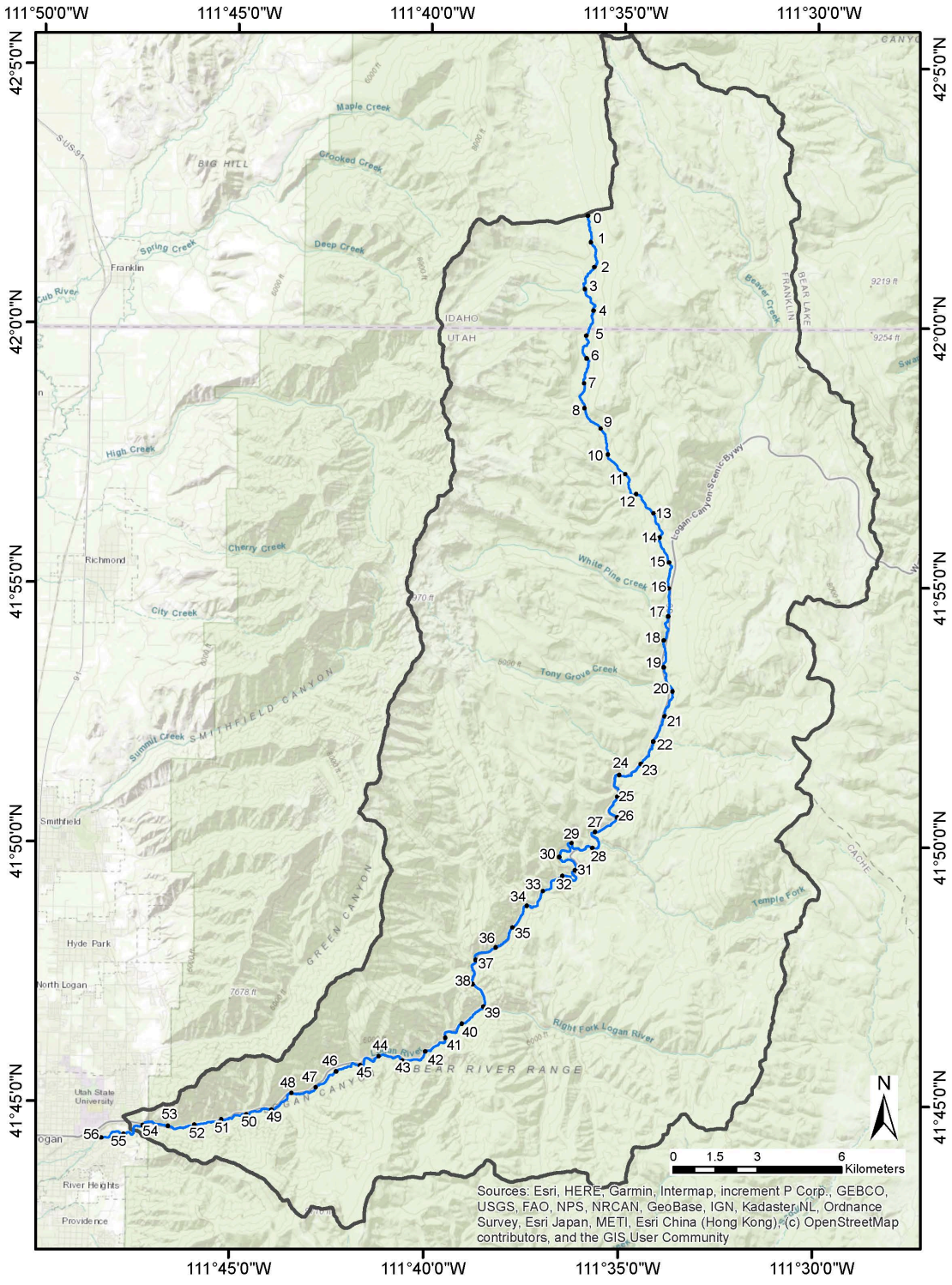

Figure 1. Map representing the Logan River Watershed. The numbered markers represent each 1-km reach.

A

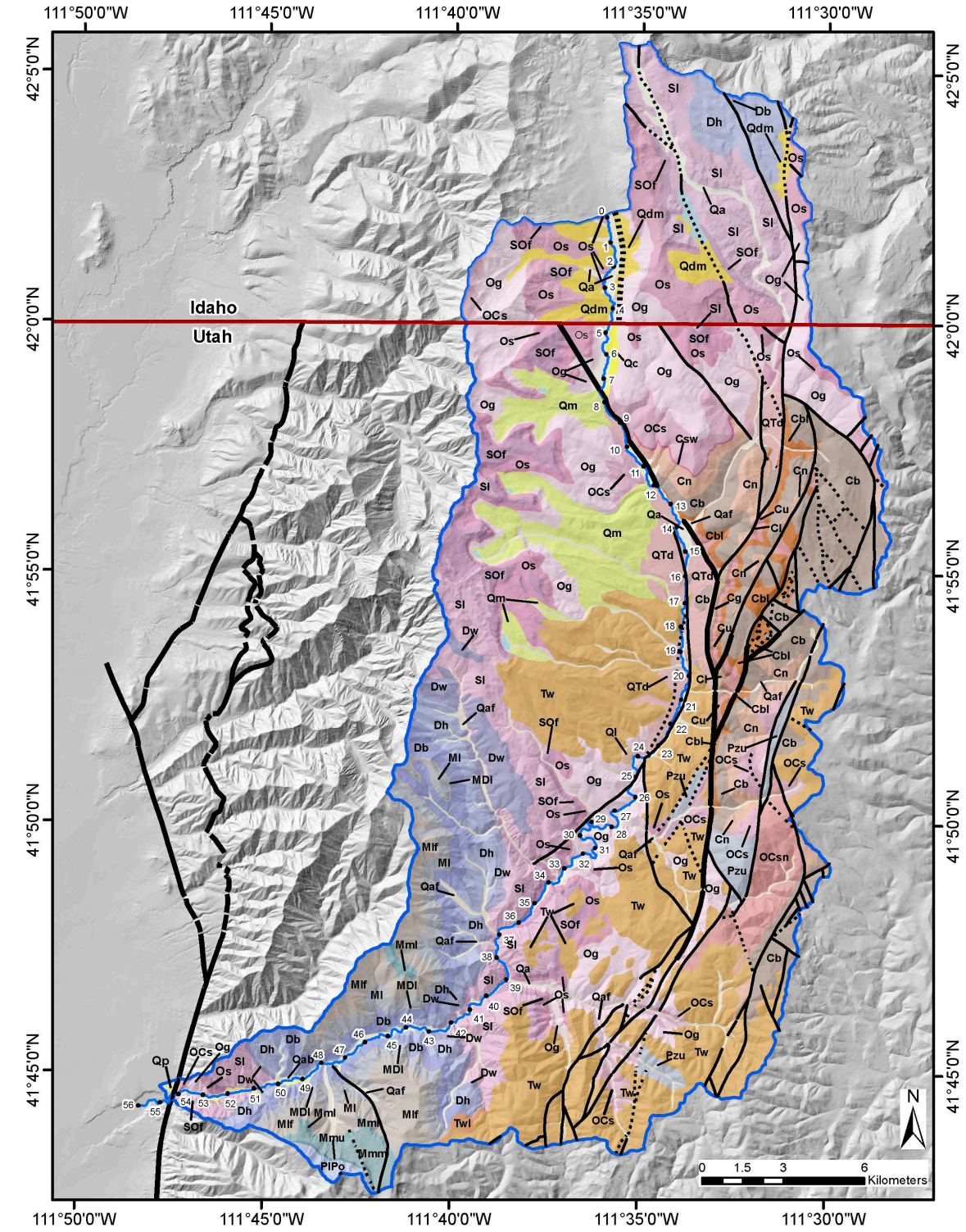
111°50'0"W
111°45'0"W
111°40'0"W
111°35'0"W
111°30'0"W
42°5'0"N
42°0'0"N
41°55'0"N
41°50'0"N
41°45'0"N
Idaho
Utah
N
0 1.5 3 6
Kilometers

B

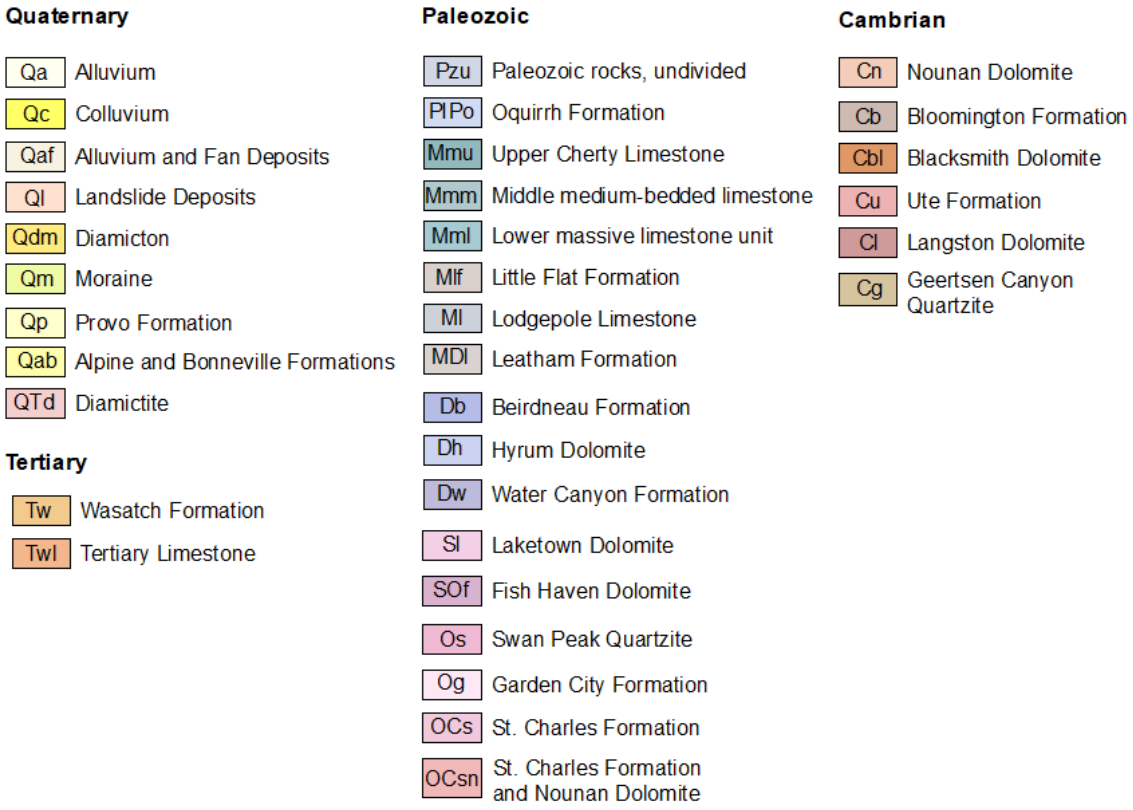

Figure 2. A) Map representing the geology of the Logan River Watershed. Thicker black lines represent potentially active normal faults associated with the Logan River. Thinner black lines represent other faults within the watershed. The red line represents the Utah-Idaho state border. B) Legend of the geologic units. Mapping and units are compiled from Dover (1995) from UGS GIS portal and Oriel and Platt (1980) from the Idaho Geological Survey.

At river-km 24, the river canyon narrows and becomes entrenched in Ordovician bedrock of the Garden City Formation, and its confluence with Temple Creek is at river-km 27. From river-km 27 to 34, the river follows a bedrock-entrenched meander pattern and flows through an increasingly deep canyon. After river-km 34, the river becomes straighter and transitions to Silurian bedrock of Laketown Dolomite. The major

Righthand Fork tributary joins the Logan River at river-km 39. The bedrock type becomes increasingly younger as the Logan River approaches the Logan Peak syncline. At river-km 43 km, the river encounters Devonian bedrock of the Beirdneau Formation, Hyrum Dolomite, and the Water Canyon Formation (Fig. 2). These rocks are composed of limestone, dolostone, and interbeds of sandstone. Additionally, the higher walls of the deep canyon consist of Mississippian and Pennsylvanian age rocks. The Logan River crosses the axis of the Logan Peak syncline at river-km 46–47, and the bedrock becomes increasingly older toward the canyon mouth after the river flows beyond the syncline.

Finally, at river-km 50, the river approaches the mountain front through Silurian and some Ordovician bedrock. As the river approaches the mountain front, the canyon becomes narrower and the fault zone including a thrust fault and the East Cache Fault (ECF) are encountered. After the river exits the mouth of the Logan Canyon at river-km 55, it encounters Pleistocene deposits of Lake Bonneville and younger basin sediments consisting of gravel, sand, silt, and clay.

Research Design

The overall approach of this study is to document and explore the patterns of the Logan River through metrics gained using GIS tools. The products include five datasets along the river profile: geologic units, river sinuosity, stream gradient, floodplain (or canyon-bottom) width, and unit stream power of the Logan River.

Data and Software

Geologic units, geolines, and geologic maps were obtained from the Utah Geological Survey (UGS). Stream shapefiles and a 10-meter digital elevation model (DEM) were acquired from Utah Automated Geographic Reference Center (UAGRC) and the United States Geological Survey, respectively. The 10-m DEM was used with ArcHydro and other geoprocessing tools to determine channel gradient, flow accumulation, and floodplain width. Valley discharge data from the Logan River Observatory and USGS were used to estimate the 2-year flood discharge (Q_2) at three gage sites along the Logan River mainstream. With these datasets, sinuosity and unit stream power along the Logan River were calculated in ArcMap and Excel.

Sinuosity

The sinuosity of a river is the channel length compared to the length of a centerline along the valley over a given reach.

$$\text{Sinuosity} = \frac{\text{Channel Length}}{\text{Length of Valley}} \qquad (1)$$

River sinuosity is usually controlled by the sediment load, gradient, and bank cohesion of a meandering river. But the Logan River is not a regular meandering stream, and it instead has bedrock-entrenched meanders. The river channel is incised through bedrock and the meanders are inherited from a prior chapter of river history. Factors that control or vary with incised meanders including channel gradient, drainage area, bedrock type, and bedrock structure. Sinuous portions of incised rivers in the Colorado Plateau are most often formed in reaches with currently low channel gradient (Harden, 1990). Gardner (1975) characterizes four general circumstances of incised rivers: 1) superimposed meanders that develop on a low-relief surface, 2) deformed incised meanders that develop on bedrock surfaces that slope upstream, 3) ingrown meanders that form in areas of lateral variation of bedrock resistance to erosion, and 4) straighter incised meanders that form on bedrock surfaces that slope in the same direction of the stream flow. An ingrown meander is an incised river with a gentle slope on one side and a steep slope on the other side. A deformed meander is an incised river where the meander bends have been eroded away as a result of shear stress caused by high velocity gradients.

Two shapefiles were used to estimate the sinuosity of the Logan River along 1 km reaches. To create a straighter valley-length shapefile, the *Draw* tool was used to trace a line through the central trend of the canyon. The line was then converted to a shapefile (displayed as a red line in Fig. 3). The stream shapefile (shown as a blue line in Fig. 3) of the Logan River was used for the channel length and was segmented into 1 km reaches according to 1 km marker points along the line using the *Split* tool. The valley length shapefile was also segmented by the *Split* tool at locations along the line that are parallel

to the 1 km markers on the stream shapefile. The sinuosity for each 1 km reach was calculated using the *Field Calculator* and exported to excel.

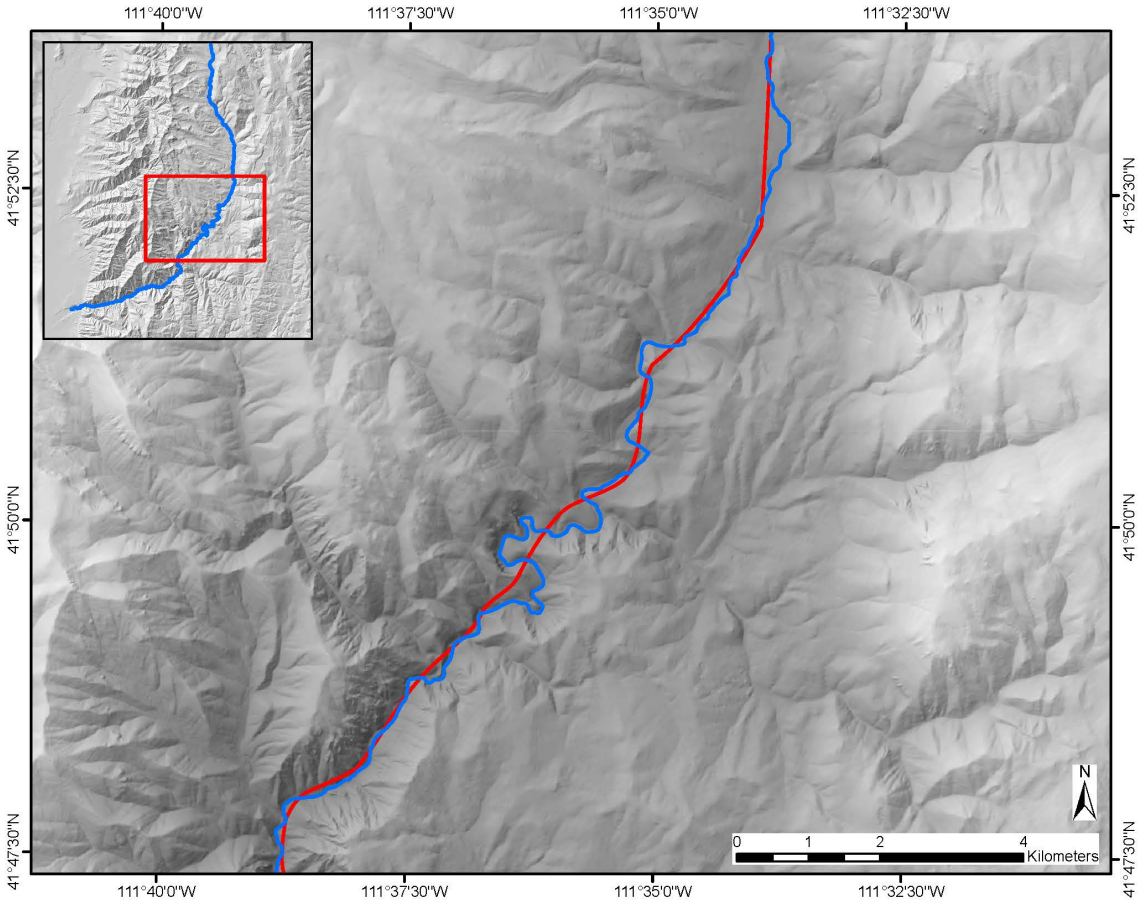

Figure 3. Map example of the two shapefiles used to determine the Logan River sinuosity around the entrenched-meander reach. The blue line represents the modern channel and its length, and the red line represents the length drawn along the central trend of the greater canyon.

Unit Stream Power

One of the most useful metrics in understanding larger-scale patterns of fluvial systems is stream power. Stream power is defined as the rate of expenditure in potential energy as a river flows against its banks and bed. Unit stream power is a measure of the

river's stream power per unit area of the channel bed obtained by dividing by width. In this case where we are asking large-scale geologic questions, the full floodplain width (w), or the canyon-bottom width, is used instead of channel width. In conducting the calculation, the density of water (ρ) is 1000 kg/m^3 and the gravity acceleration constant (g) is 9.8 m/s^2. Having the necessary components, the unit stream power (Ω_u) for each 1 km reach is calculated using the following equation:

$$\Omega u = \frac{\rho g Q S}{w} \qquad (2)$$

Discharge

Discharge data were obtained from the Logan River Observatory and the United States Geological Survey (USGS), collected from three gages along the Logan River. Two are located upstream at Franklin Basin and Tony Grove at river-km 11 and 21, respectively. The USGS gage site is located downstream near First Dam at river-km 54. The Logan River Observatory has 15-minute discharge data from 2014 to 2015 for five of the gage sites and the USGS gage has daily average discharge data from 1986 to 2020.

To calculate the two-year flood frequency for each gage site, a Pearson Type III standard calculation was conducted. The discharge data first had to be re-organized from the 15-minute interval to the maximum flow for each of the five years. After listing the peak flow values for each year, the values were first log-transformed in order to normalize the data. Next, the mean (M), standard deviation (S), and skew coefficient of the log-transformed values were calculated. Using the skew coefficient, the frequency

factor (K) for the 2-year flood was determined using a Pearson Type III Distribution table (Mays, 2005). Knowing the frequency factor, the log mean, and the log standard deviations, the 2-year flood discharge (Q_2) was calculated for all three gage sites by

$$Q_2 = 10^{M + K* S} \quad (3)$$

To interpolate the discharge every 50 meters downstream so that unit stream power could be determined along the entire river, the Q_2 for gage sites were plotted against the distance downstream and the least-squares best fit line was determined as

$$Q_2 = 0.3241x + 4.23 \quad (4)$$

Using equation 4., Q_2 was calculated every 50 m downstream across the study reaches.

A common alternative to determining discharge based on real-world data, is substituting contributing area assuming each unit of area contributes the same amount of Q_2. Contributing area values along the Logan River were calculated from flow accumulation values. The *Flow Accumulation* tool calculates the accumulated number of raster cells that flow to a given pixel via flow direction. To calculate the river's contributing area every 1 km downstream, flow accumulation values along the river line were multiplied by the square of the DEM's cell size in Excel.

Gradient

The *Generate Points Along Line* geoprocessing tool was used to create 1 km marker points along the Logan River shapefile (shown in Figure 1). Then, the *Extract Values to Points* geoprocessing tool was used to assign elevation values from the DEM to the marker points. This was exported to Microsoft Excel using the *Table-to-Excel* tool in ArcMap. Using Excel, the gradient for each 1 km reach between 1 km-spaced points was calculated and the results were plotted.

Floodplain Width

For this study, floodplain width is being used for the unit stream power calculation rather than normal channel width for two reasons. First, high resolution DEMS are limited for most of Logan Canyon and the narrow channel cannot be resolved. Secondly, this study is asking large-scale questions and a broader geologic metric of canyon-bottom width is warranted. To estimate the floodplain or canyon-bottom width of the Logan River, a geoprocessing tool known as the *Valley Bottom Extraction Tool* (VBET) was used in ArcMap. The VBET tool was developed by William MacFarlane, Jordan Gilbert, and Dr. Joseph Wheaton of Utah State University (USU) in 2016. It creates a polygon that represents the valley bottom along a stream using two inputs, a DEM and a stream network shapefile. After the valley bottom polygon was created, the polygon was manually segmented for each 1-km reach. The *Calculate Geometry* tool was used to estimate the area of each polygon. Average widths for the Logan River floodplain were estimated every 1 km by dividing the polygon areas by their respective lengths of

1000 meters each. The *Field Calculator* in ArcMap was used to calculate the average floodplain width for each polygon.

Results and Discussion

Sinuosity

There are distinct reaches of the Logan River with entrenched meanders from km 28 to 33 (Fig. 4B). Here, the river has a sinuosity over 3 and in the central part over 1.5, which indicates a strong meandering pattern. The average sinuosity of the river is approximately 1.30 and many of the reaches fall below this value. Along most of the river's length, it has a sinuosity between 1 and 1.5 and the only real anomaly is the high sinuosity reaches at river-km 28 – 33. The reaches with the highest sinuosity correspond with the Ordovician Garden City Formation bedrock (Fig. 4A). The highest sinuosity reaches are also compared with the discharge (Fig. 5B), gradient (Fig. 5C), floodplain width (Fig. 5D) and unit stream power (Fig 5E.). The results are somewhat contrary with Gardner's (1975) findings, where incised meanders form on the upstream flank of an uplift, compressed against the rising bedrock surface, and then they tend to straighten flowing down the other side of the structural high. In the case of the Logan River, the entrenched meanders are on the upslope side of the uplifting range, but only in a discrete part of it. Since the Logan River is antecedent and older than the Bear River Range uplift, it can be deduced from the entrenched meanders that the river was more meandering in the past. Yet, over time, most reaches straightened as channel gradient became steeper, presumably due to increasing uplift to the west.

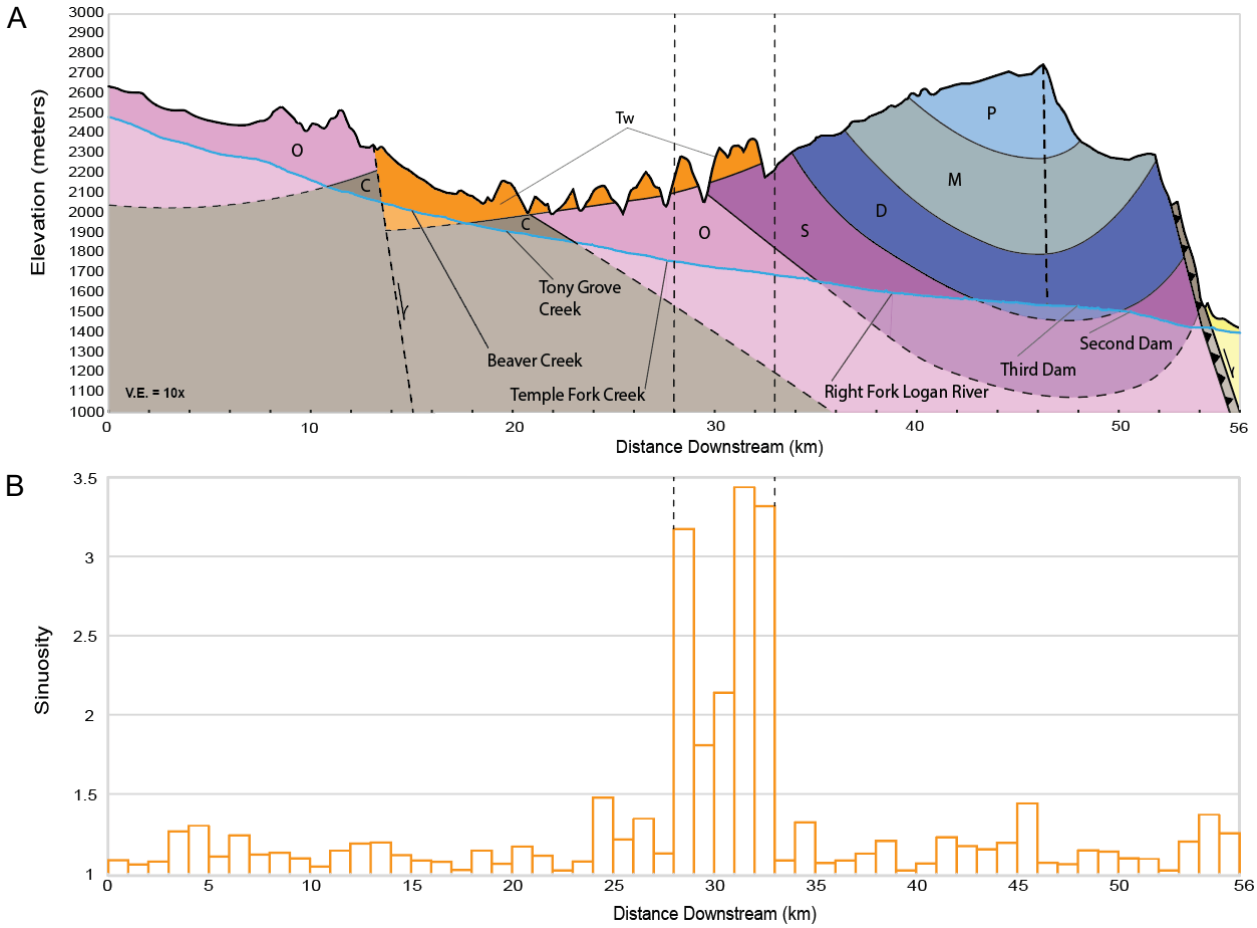

Figure 4. A) Topographic profile of the Bear River Range and long profile of the Logan River in cross-sectional view, displaying the simplified geology and major tributaries along the river's path. B) Histogram of Logan River sinuosity in 1 km reaches. The dashed lines represent the reaches of entrenched meanders.

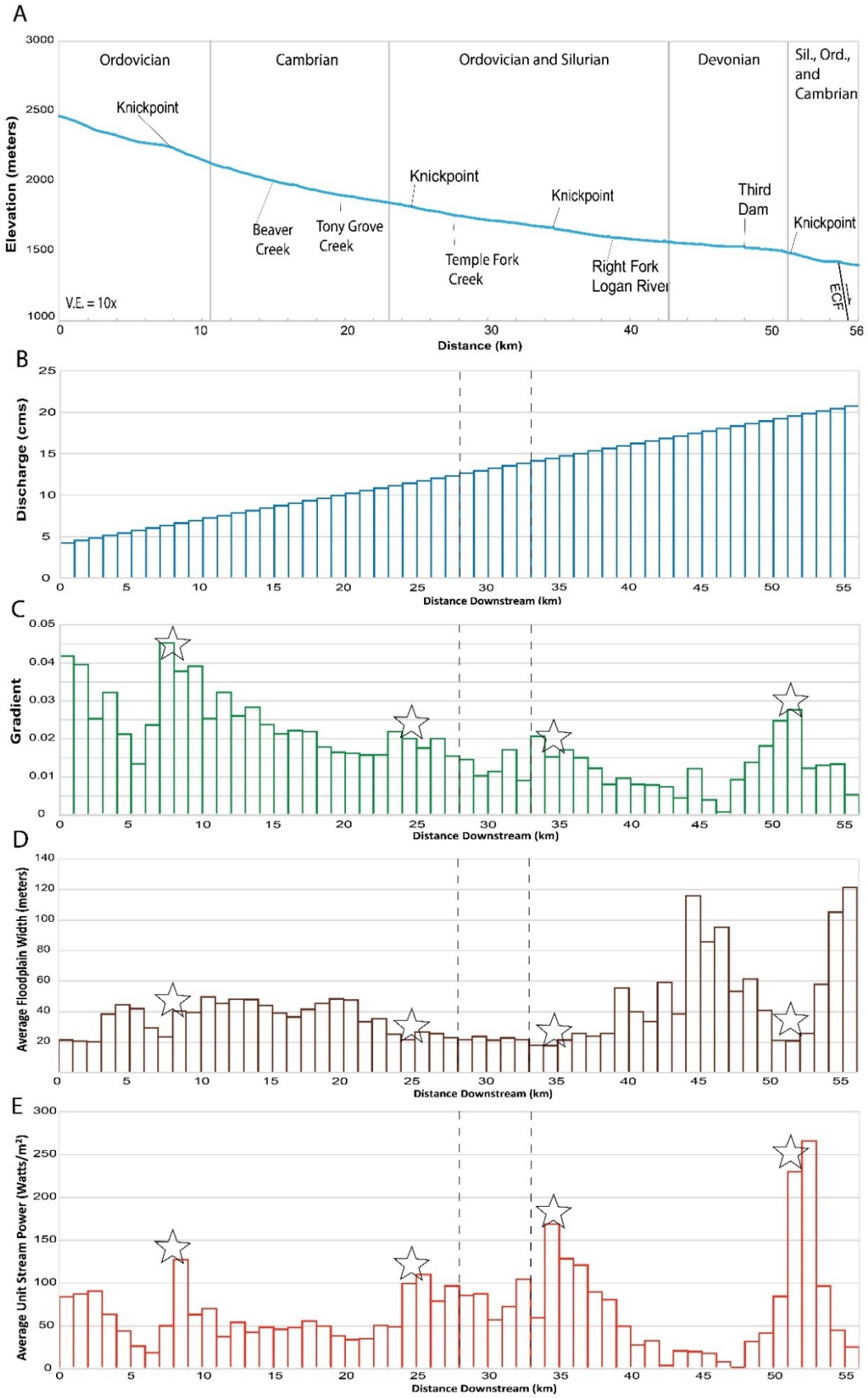
A
Ordovician
Cambrian
Ordovician and Silurian
Devonian
Sil., Ord., and Cambrian
Knickpoint
Knickpoint
Knickpoint
Third Dam
Knickpoint
Beaver Creek
Tony Grove Creek
Temple Fork Creek
Right Fork Logan River
ECF
V.E. = 10x
Elevation (meters)
Distance (km)
B
Discharge (cms)
Distance Downstream (km)
C
Gradient
Distance Downstream (km)
D
Average Floodplain Width (meters)
Distance Downstream (km)
E
Average Unit Stream Power (Watts/m²)
Distance Downstream (km)

Figure 5 (previous page). A) Elevation profile of Logan River with general bedrock age, major tributaries, and the four knickpoints labeled. B) Logan River 2-year-recurrence flood discharge for 1-km reaches. C) Channel gradient for 1-km reaches. D) Reach-average floodplain width from the VBET tool. E) Logan River reach-averaged unit stream power. Stars serve as location markers for the four knickpoints apparent in longitudinal profile. The dashed lines bracket the reaches with entrenched meanders from Fig. 4.

Discharge

The Q_2 discharge estimated for the Logan River from the three gages increases from upstream to downstream in a linear fashion, because it is based on a linear regression through the points (Table 1; Fig. 6). Roughly similar, the contributing area increase follows a linear trend, but with sudden jumps (Fig. 7), which represent the confluences of Beaver Creek, Temple Fork, and the Righthand Fork tributaries. Deviating from this linear trend, the increase in contributing area decreases notably starting at 40 km, which must represent an absence of major feeding tributaries in that lower reach. The regression from the Q_2 plot does not extend to the (0,0) origin of plot, but the contributing area plot does because the contributing area is assumed to be zero at where the river begins.

TABLE 1. 2-YEAR FLOOD DISCHARGE FOR LOGAN RIVER GAGE SITES

Site	Distance Downstream (meters)	2-Year Flood Frequency Discharge (m^3/s)
Franklin Basin	11,300	7.8
Tony Grove	21,000	11.1
USGS Gage	54,000	21.7

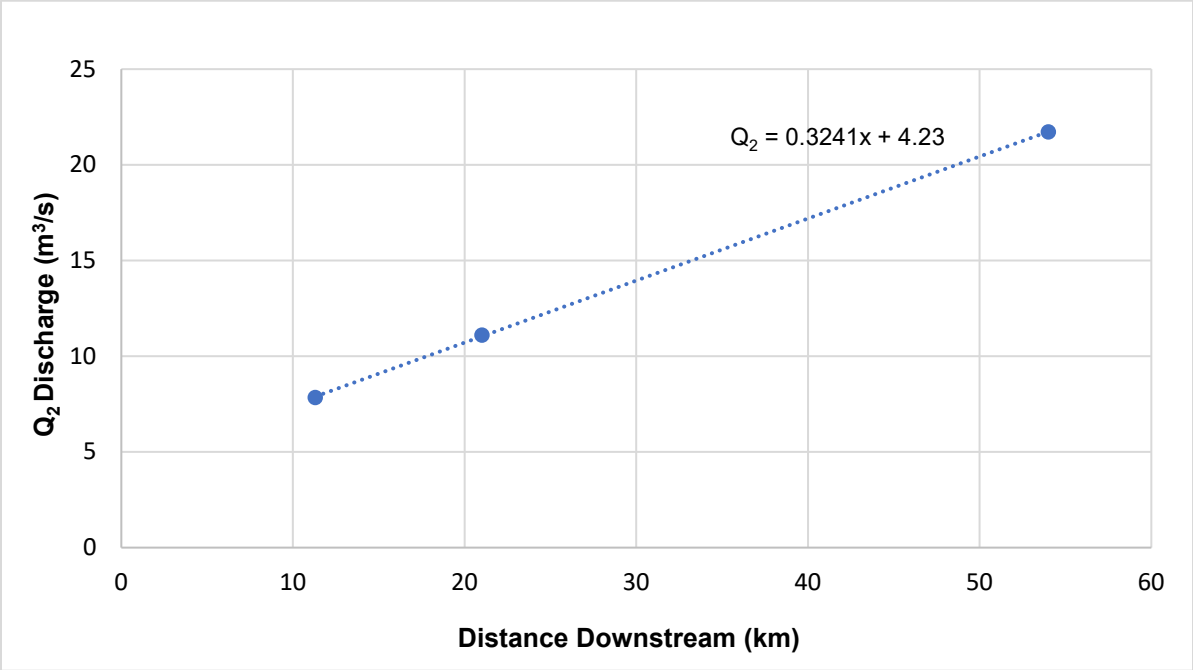

Figure 6. A graph that plots the 2-year flood discharge for gage sites at Franklin Basin, Tony Grove, and the USGS site based on the distance of their sites downstream. The trendline equation shown is used to determine the 2-year flood discharge at distances of every 1 km downstream.

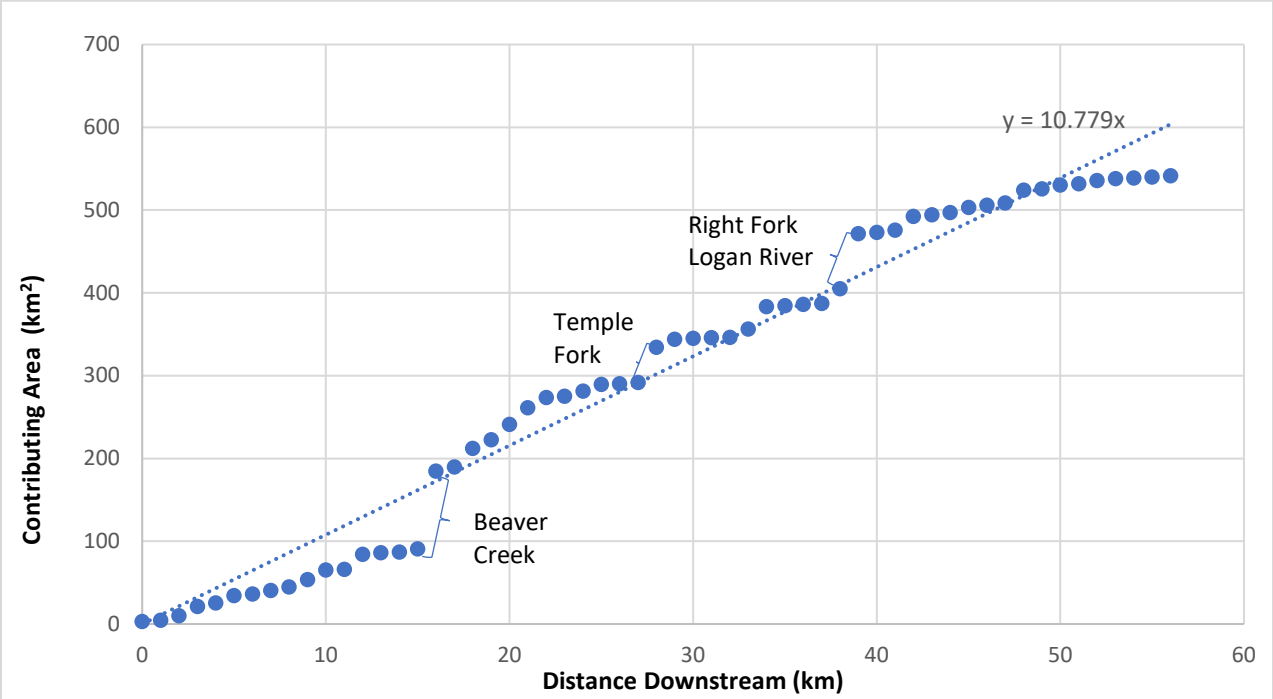

Figure 7. A plot of the Logan River's contributing area derived from the flow accumulation geoprocessing tool from ArcHydro.

Given the two linear functions from both graphs and ignoring the y-intercepts, flood runoff (Q_2) can be estimated from contributing area (A):

1) $Q_2 = 0.3241 * D \quad \Rightarrow \quad D = \frac{Q2}{0.3241}$

And

2) $A = 10.78 * D$

Then, rearranging equation 1 to solve for D, and substituting that into equation 2 gives:

3) $A = 10.78 * \frac{Q2}{0.3241} \quad \Rightarrow \quad A = 33.26 * Q_2$

$\Rightarrow \quad Q_2 = 0.03 * A$

This indicates that each 1 km^2 of contributing area provides to the Q_2 flood an average of ~0.03 m^3/s, which is equivalent to ~1 ft^3/s of flood runoff over the Logan River basin.

There are advantages and drawbacks inherent in both approaches in estimating discharge along the river's length. An advantage of the Q_2 from gage stations is that it is based on real-world data. However, the disadvantages are that discharge data are interpolated across only three gage sites, producing a linear trend of increasing discharge that is certainly too simple in pattern, and that they were collected over a short time interval. Therefore, the data are only valid for a two-year flood frequency as opposed to a long-term prediction. The advantage of the contributing-area approach is that it is useful for when real discharge data are limited and can be used to justifiably estimate discharge at any point along the river rather than only at limited gauge sites. However, the disadvantage of this method is the primary assumption that there is a fixed amount of discharge being added to the river by overland flow for every square area of the watershed when there may actually be more or less runoff generated across different areas of the catchment.

Floodplain Width

The floodplain width along the Logan River as delineated by the VBET tool has a mean width of 40 m. The floodplain width is widest at reach-km 44-48 and 53-55, and narrowest at reach-km 0-3, 6-9, 21-38, and 50-52 (shown in Fig. 5D and Fig 8.). The reaches with the narrowest floodplain widths coincide with reaches that have high gradient and unit stream power, while the reaches with wider floodplain width are associated with low gradient and lower unit stream power. Also, there appears to be an association between the narrowest floodplain widths and Silurian and Ordovician bedrock units Laketown Dolomite, Fish Haven Dolomite, and Swan Peak Quartzite at reach-km 0-3, 33-35, and 50-52.

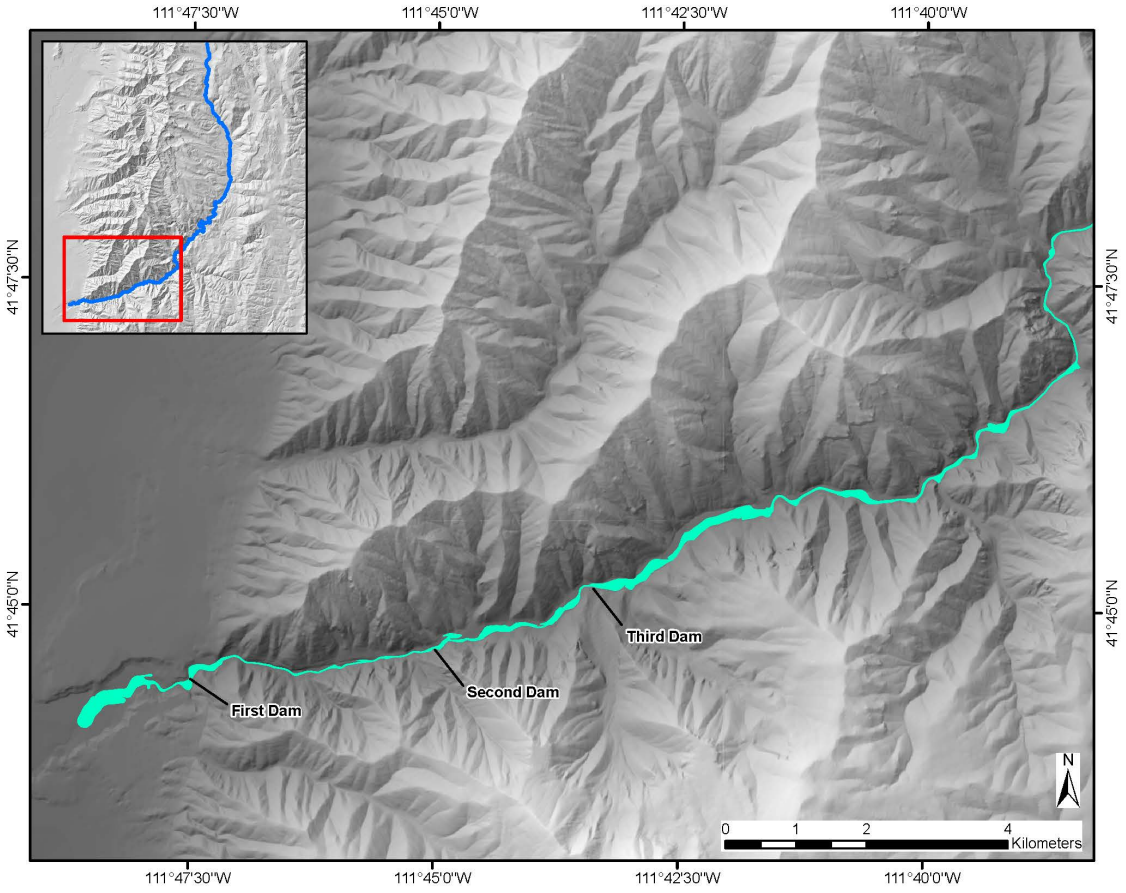

Figure 8. Map of lower Logan Canyon results for floodplain area produced from the Valley Bottom Extract Tool (VBET).

As the Logan River exits the entrenched meander, the river becomes straightened and wider especially below the confluence with Righthand Fork (reach-km 44-48) as it flows downstream while still approaching the fastest uplifting, western edge of the range. The river becomes wide above third dam starting at river-km 45. This is unexpected since it was exceptionally wider than any reach upstream and is almost as wide as the river is down in Cache Valley basin where there is no bedrock uplift. As the river crosses the Logan Peak syncline, starts encountering older bedrock and approaches the uplifting

mountain front, it narrows and the stream power increases to keep up with the uplift (reach-km 50-53). The Logan River canyon-bottom then becomes wide after the mouth of the canyon at reach-km 54 because the gradient becomes less steep, it is flowing through unlithified Lake Bonneville sediment, and it is no longer experiencing uplift after it crosses the East Cache fault. The wider canyon bottoms are not a result of anthropogenic reservoirs and dams. The VBET tool minimizes the effect of reservoirs because it only uses a line shapefile input and does not use waterbody shapefile inputs in the tool's geoprocessing analysis. Also, only third dam is located in the anomalously wide reach, while first and second dams are downstream. And the wide reach above third dam continues 3 kilometers upstream of the reservoir, which the third dam is incapable of doing.

Gradient and Unit Stream Power

For the Logan River, gradient does not smoothly decrease as it theoretically should for a graded, equilibrium stream (Fig. 5C). The mean gradient for the Logan River is 0.019 and the gradient deviates lower from this value downstream at reach-km 27-33, 37-47, and 52-56. For unit stream power, results indicate average unit stream power along the Logan River is 67.2 watts/m^2, but it is highly variable and reaches a huge peak of nearly 300 watts/m^2 in the prominent knickzone just above the mouth of the canyon and the mountain front of the Bear River Range (Fig. 5E). There are four notable knickzones where the gradient and unit stream power peak -- in reach-kms 8-10, 24-26, 34-35, and 51-53. Three of the knickzones coincide with Ordovician strata while one coincides with Silurian (Fig. 4A and 5C). Comparing Figures 4B and 5C, the knickzones

coincide with reaches that have relatively low sinuosity. Furthermore, the reaches with high unit stream power coincide with both high gradient and low floodplain width. The first, farthest upstream knickzone at 8-10 km flows through Quaternary till deposits of glacial end moraines. The knickpoint at this reach may be caused by the river crossing these coarse deposits. The middle two knickzones at 24-25 km and 34-35 km are not near active faults, and the cause for these two knickzones is not clear. The most prominent knickzone at reach-km 51-53, approaching the mouth of Logan Canyon, lies just upstream of the active ECF and therefore could be caused by it. A visual overhead view of the river's unit stream power is shown in Figure 9.

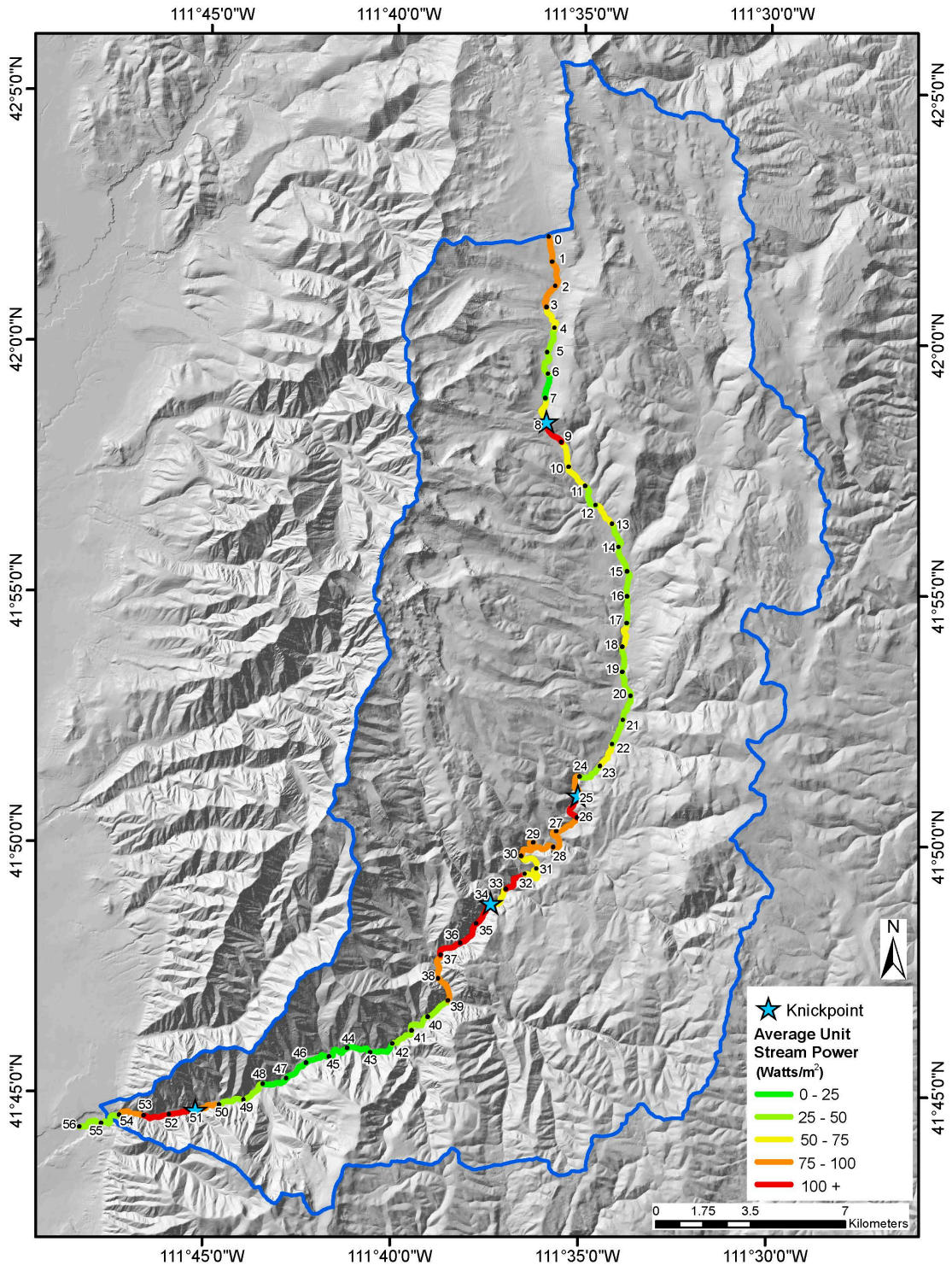

Figure 9. Map displaying the 1 km-reach-average unit stream power along the Logan River.

There are three possible explanations for why the middle two knickpoints occurred. The first is that they formed as a result of tectonic uplift from the ECF and have migrated upstream over time. According to Oaks and Runnells (1992), there are faults located around the entrenched meander reaches, but they are not likely active and probably not the cause for the formation of the middle two knickpoints located at the beginning and end of the entrenched meander. The second explanation is that they formed as a result of difference in bedrock type and tensile strength. There is no data available to really assess the strength of these bedrock units for this study. However, this option seems unlikely given that the Ordovician and Silurian strata are primarily limestone and dolostone, except the lower 200 meters of the Ordovician Swan Peak Formation, which is shale (Hintze, 2005). A previous analysis of the Logan River longitudinal profile by DeGraff (1976) likewise indicated that there is no clear correlation between bedrock lithology and changes in gradient, with the caveat that one convexity appeared to be associated with Swam Peak Formation. The third explanation is that these knickpoints could be formed by debris from a major mass-movement, such as a landslide. This study does not include ground-truthing field surveys, which are necessary to determine whether or not this may be the cause of the knickpoints.

At the start of this chapter, research questions were posed about the sinuosity, stream power, gradient, canyon-bottom width of the Logan River and their correspondence to bedrock type. Questions were also posed about the causes of high gradient and unit stream power along the course of the river. The hypothesis of this exercise was that unit stream power is greatest in reaches associated with tectonic uplift and hard bedrock and lowest in reaches with weaker bedrock and broader canyon-bottom

width. In summary, the analyses indicate that bedrock type has no correspondence with sinuosity, unit stream power, gradient, and canyon-bottom width. The analyses also show that unit stream power and gradient are highest at four knickzones throughout the Logan River main stem. Unit stream power is exceptionally highest at the knickzone located at the mountain front upstream of the tectonically active ECF and lowest in the reaches with broader canyon-bottom widths. Therefore, the analyses show that the hypothesis of this exercise is indeed correct.

CHAPTER 4

SUMMARY

The use of GIS gives many advantages of conducting these exercises that answers the research questions of these studies in a more efficiently and timely manner. GIS can provide visuals of paleosurfaces and the ECF planar surface, both of which can almost not be accomplished manually. The interpolations used in the first exercise involve the use of complex algorithms that are too difficult and time consuming to estimate without the use of GIS. Total slip and Fault plane surface area are typically estimated using quantitative evaluation of slip parameters in geophysics but can also be answered using 3D modeling if data is significantly accurate. Estimating the total displacement, surface area, and earthquake metrics of the ECF in relation to the paleosurfaces would be almost impossible to accomplish without GIS. In the case of the Logan River exercise, river metrics such as gradient, sinuosity, floodplain width, and stream power throughout a river network can all be determined without GIS using field-surveys, but it would require a vast amount of time. DEMs and remote sensing make it easier to estimate river metrics quicker and more efficiently. GIS can provide visuals and maps that help observe specific patterns and correlations of river metrics. Without GIS, several phases of these exercises would require more work, resources, and time.

For these two exercises, there are certain aspects that can be improved or done differently. In creating the paleosurfaces, more interpolation points could provide a more detailed and accurate appearance. Rather than having the ECF as one segment, the analyses can be conducted on multiple segments including the north, south, and central

segments of the ECF. The varying fault dip angles affiliated with each of these segments should be used in further analyses. The ECF analyses should also take multiple earthquake events into account rather than treating the creation of the ECF as just one single event. For the Logan River exercise, the river might be studied over smaller-scale reaches, such as every 50 or 100 m instead of 1 km. Studying the river over shorter reaches would provide more details of where sinuosity, gradient, width, and stream power are highest and lowest. Results in this exercise are based more upon visual interpretation to correlate river metrics, knickzones, and bedrock type. In further studies, geostatistical analyses can be used to provide numerical estimates of correlation in river metrics, patterns, knickzones, and bedrock type. To understand more on what causes the four knickzones in the longitudinal profile of the Logan River, fieldwork and ground-truth field surveys can be conducted to provide additional evidence.

REFERENCES CITED

Childs, C., 2004, Interpolating Surfaces in ArcGIS Spatial Analyst: Arc User, p. 32 – 35.

DeCelles, P.G., 1994, Late Cretaceous–Paleocene synorogenic sedimentation and kinematic history of the Sevier thrust belt, northeast Utah and southwest Wyoming: *Geological Society of America Bulletin*, v. 106, p. 32–56.

DeGraff, J.V., 1976, Quaternary Geomorphic Features of the Bear River Range, North-Central Utah [M.S. Thesis]: Utah State University, 199 p.

Dover, J.H., 1995, Geologic map of the Logan 30′ × 60′ quadrangle, Cache and Rich counties, Utah, and Lincoln and Uinta counties, Wyoming: U.S. Geological Survey Miscellaneous Investigations Series Map I-2210, scale 1:100,000. 3 plates.

Evans, J.P., and Oaks, R.Q., Jr., 1996, Three-dimensional variations in extensional fault shape and basin form: The Cache Valley basin, eastern Basin and Range province, USA: Geological Society of America Bulletin, v. 108, p. 1580-1593.

Gardner, T.W., 1975, The history of part of the Colorado River and its tributaries-an experimental study: Four Corners Geological Society Field Conference. 8th. Guidebook. p. 87-95.

Gutenberg, B., and Richter, C.F., 1944, Frequency of earthquakes in California: Bulletin of the Seismological Society of America. v. 34, p. 185-188.

Hanks, T.C., and Kanamori, H., 1979, A moment magnitude scale: Journal of Geophysics, Res. 84, p. 2348-2350.

Hintze, L.F., 2005, Utah's Spectacular Geology: Department of Geology, Brigham Young University.

Harden, D.R., 1990, Controlling factors in the distribution and development of incised meanders in the central Colorado Plateau: Geological Society of America Bulletin, v. 102, p. 233-242.

Mackin, J., 1948, Concept of the graded river: Geological Society of America Bulletin, v. 48, p. 463-512.

Mays, L.W., 2005, Water Resources Engineering: John Wiley & Sons. 928 p.

McCalpin, J.P., and Forman, S.L., 1991, Late Quaternary faulting and thermoluminescence dating of the East Cache fault zone, north-central Utah: Bulletin of the Seismological Society of America, v. 81, no. 1, p. 139 – 161.

McCalpin, J.P., and Forman, S.L., 1994, Neotectonic deformation along the East Cache fault zone, Cache County, Utah: Utah Geological Survey Special Study 83, 37 p.

Oaks, R. Q., Jr., and Runnells, T. R., 1992, The Wasatch Formation in the central Bear River Range, northern Utah: Utah Geological Survey Contract Report 92-8, 79 p., 7 plates.

Oriel, S.S., and Platt, L.B., 1980, Geologic map of the Preston 1° × 2° quadrangle, southeastern Idaho and western Wyoming: U.S. Geological Survey Miscellaneous Investigations Series Map I-112, scale 1:250,000. 1 plate.

Schwartz, D.P., and Coppersmith, K.J., 1984, Fault behavior and characteristic earthquakes: examples from the Wasatch and San Andreas fault zones: Journal of Geophysical Research, v. 89, p. 5681-5698.

Stein, R.S., and Barrientos, S.E., 1985, Planar high-angle faulting in the Basin and Range: Geodetic analysis of the 1983 Borah Peak, Idaho, earthquake: Journal of Geophysical Research, v. 90, p. 1355–1366.

Turcotte, D.L., and Schubert, G., 2002, Geodynamics: Cambridge University Press. 848 p.

Zuchiewicz, W., and Oaks R.Q. Jr., 1993, Geomorphology and structure of the Bear River Range, NE Utah: a morphometric approach: Zeitschrift für Geomorphologie, Suppl. Bd., n. 94, p. 41-55.